

AD-A084 339

COLORADO STATE UNIV FORT COLLINS FLUID MECHANICS AND--ETC F/6 20/4  
DISPERSION OF VAPOR FROM LNG SPILLS -- SIMULATION IN A METEOROL--ETC(U)  
MAR 79 D E NEFF, R N MERONEY DOT-CG-75279-A

UNCLASSIFIED

USCG -D-15-80

NL

1 of 1  
AD  
A084339

END  
DATE  
FILMED  
6-80  
DTIC

ADA084339

FINAL REPORT

MARCH 1978

Document is available to the public through the  
National Technical Information Service,  
Springfield, Virginia 22161

Prepared for

U.S. DEPARTMENT OF TRANSPORTATION  
United States Coast Guard  
Office of Research and Development  
Washington, D.C. 20590

80 5 15 02.9

1. Report No. <b>18</b> US CGD-15-80	2. Government Accession No. <b>19</b> AD-A084 339	3. Recipient's Catalog No.	
4. Title and Subtitle <b>6</b> DISPERSION OF VAPOR FROM LNG SPILLS -- SIMULATION IN A METEOROLOGICAL WIND TUNNEL OF SPILLS AT CHINA LAKE NAVAL WEAPONS CENTER, CALIFORNIA		5. Report Date <b>11</b> March 1979	6. Performing Organization Code
7. Author(s) <b>10</b> D. E. Neff and R. N. Meroney		8. Performing Organization Report No.	9. Postmaster: Report No.
10. Performing Organization Name and Address Fluid Mechanics and Diffusion Laboratory Department of Civil Engineering Colorado State University Fort Collins, Colorado 80523		11. Work Unit No. (TRIS)	12. Contract or Grant No.
12. Sponsoring Agency Name and Address Commandant (G-DMT-1/54) U.S. Coast Guard Headquarters Washington, D. C. 20593		13. Type of Report and Period Covered <b>15</b> DOT-CG-75279-A	14. Sponsoring Agency Code
15. Supplementary Notes			
<p>16. Abstract</p> <p>Physical simulation of a series of four, six cubic meter Liquefied Natural Gas (LNG) spills on water was provided by the Meteorological Wind Tunnel facilities at Colorado State University. Field data were collected from spills performed at Naval Weapons Center, China Lake, California, in Fall 1978. The simulation test series was to provide field test planning information, extend the value of a limited set of field measurements, and validate the concept of physical modeling of LNG plume dispersion as a predictive hazard analysis tool.</p> <p>Two test series were conducted to aid in placement of field concentration measurement instrumentation. The first utilized 1:170 scale model of the China Lake site in the Meteorological Wind Tunnel and the second utilized 1:85 scale model in the Environmental Wind Tunnel. Dispersion data collected in the four field tests at China Lake were extended in two test series conducted in the Environmental Wind Tunnel over a 1:85 scale model. The following results were obtained:</p> <p>(1) Comparison between dispersion data for similar test parameters but at two different model scales, 1:85 and 1:170 produces similar concentration variation.</p> <p>(2) The China Lake surface roughness and topography causes the LNG vapor plume to disperse more rapidly than would be experienced over flat terrain.</p> <p>(3) For the four simulated LNG field tests the arrival time, peak concentration, maximum peak, etc., have been tabulated; peak ground level concentration contours have been determined; and normalized peak concentration coefficients vs. downwind distance have been plotted.</p>			
17. Key Words LNG Wind Tunnel Vapor Dispersion Atmospheric Modeling		18. Distribution Statement This document is available to the U.S. public through the National Technical Information Service, Springfield, Virginia 22161	
19. Security Classif. (of this report) Unclassified	20. Security Classif. (of this page) Unclassified	21. No. of Pages 90	22. Price

A

S/

088320

y/p

# METRIC CONVERSION FACTORS

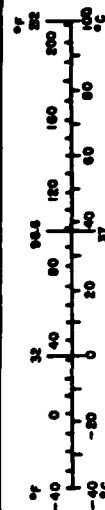
## Approximate Conversions to Metric Measures


Symbol	When You Know	Multiply by	To Find	Symbol
<b>LENGTH</b>				
in	inches	2.5	centimeters	cm
ft	feet	30	centimeters	cm
yds	yards	0.9	meters	m
mi	miles	1.6	kilometers	km
<b>AREA</b>				
sq in	square inches	6.5	square centimeters	cm <sup>2</sup>
sq ft	square feet	0.09	square meters	m <sup>2</sup>
sq yds	square yards	0.8	square meters	m <sup>2</sup>
sq mi	square miles	2.6	square kilometers	km <sup>2</sup>
acres	acres	0.4	hectares	ha
<b>MASS (weight)</b>				
oz	ounces	28	grams	g
lb	pounds	0.45	kilograms	kg
	short tons (2000 lb)	0.9	tonnes	t
<b>VOLUME</b>				
teaspoon	teaspoons	5	milliliters	ml
Tablespoon	tablespoons	15	milliliters	ml
Fluid ounce	fluid ounces	30	milliliters	ml
Cup	cups	0.24	liters	l
Pint	pints	0.47	liters	l
Quart	quarts	0.95	liters	l
Gallon	gallons	3.8	liters	l
Cubic foot	cubic feet	0.03	cubic meters	m <sup>3</sup>
Cubic yard	cubic yards	0.76	cubic meters	m <sup>3</sup>
<b>TEMPERATURE (exact)</b>				
°F	Fahrenheit temperature	5/9 (after subtracting 32)	Celsius temperature	°C

\* 1 in = 2.54 (exactly). For other exact conversions and more detailed tables, see NBS Misc. Publ. 286, Units of English and Metric Measures, Price \$2.25, SD Catalog No. C13.10-286.

## Approximate Conversions from Metric Measures

When You Know	Multiply by	To Find	Symbol
<b>LENGTH</b>			
millimeters	0.04	inches	in
centimeters	0.4	inches	in
meters	2.2	feet	ft
meters	1.1	yards	yds
kilometers	0.6	miles	mi
<b>AREA</b>			
square centimeters	0.16	square inches	in <sup>2</sup>
square meters	1.2	square yards	yd <sup>2</sup>
square kilometers	0.4	square miles	mi <sup>2</sup>
hectares (10,000 m <sup>2</sup> )	2.5	acres	ac
<b>MASS (weight)</b>			
grams	0.005	ounces	oz
kilograms	2.2	pounds	lb
tonnes (1000 kg)	1.1	short tons	ton
<b>VOLUME</b>			
milliliters	0.03	fluid ounces	fl oz
liters	2.1	pints	pt
liters	1.05	quarts	qt
liters	0.26	gallons	gal
cubic meters	35	cubic feet	ft <sup>3</sup>
cubic meters	1.3	cubic yards	yd <sup>3</sup>
<b>TEMPERATURE (exact)</b>			
Celsius temperature	9/5 (then add 32)	Fahrenheit temperature	°F



Accession For	
NTIS GRA&I	
DDC TAB	
Unannounced Justification	
By _____	
Distribution/	
Availability Codes	
Dist.	Avail and/or special
A	

DTIC  
ELECTE  
MAY 19 1980  
S D

## EXECUTIVE SUMMARY

As part of a program to evaluate the hazards associated with

Liquid Natural Gas (LNG) spills a series of six cubic meter LNG spill tests were performed at China Lake Naval Weapons Center. Simultaneously, physical simulation of these spills were provided by the meteorological wind tunnel facilities at Colorado State University. The intent of the simulation test series was to provide field test planning information, to extend the value of a limited set of field measurements, and to validate the concept of physical modeling of LNG plume dispersion as a predictive hazard analysis tool.

Two test series were conducted during the preliminary investigations to guide the placement of field instrumentation. The first series utilized a 1:170 scale model of the China Lake site in the Colorado State University Meteorological Wind Tunnel; whereas the second series incorporated a 1:85 scale model in the CSU Environmental Wind Tunnel. Subsequently two test series were performed over a 1:85 scale model in the Environmental Wind Tunnel to extend dispersion data for four field tests; China Lake LNG-18, LNG-19, LNG-20, and LNG-21. These test programs provide the following results:

- 1) A comparison between dispersion data for similar test parameters but at two different model scales, 1:85 and 1:170 produces similar concentration variation.
- 2) The China Lake surface roughness and topography causes the LNG vapor plume to disperse more rapidly than would be experienced over flat terrain.

- 3) The arrival time, peak concentration, maximum peak, etc. have been tabulated together for the four simulated LNG field tests.
- 4) Peak ground level concentration contours are provided for the four simulated LNG field tests.
- 5) Normalized peak concentration coefficients with respect to downwind distance are plotted for the four simulated LNG field tests.

#### ACKNOWLEDGMENT

The authors wish to acknowledge the fiscal support of the U. S. Coast Guard, Department of Transportation Contract DOT-CG-75279-A. The successful completion of this work depended on the encouragement of Dr. R. DeVore, American Gas Association, and Dr. J. Cece, Department of Energy; the co-ordination and consideration provided by Lt. G. Colonna, U.S. Coast Guard, and the scientific stimulation and cooperation of Dr. Doug Lind, China Lake Naval Weapons Center, and Dr. William Hogan and his staff at Lawrence Livermore Laboratory, California.

## TABLE OF CONTENTS

<u>Chapter</u>		<u>Page</u>
	EXECUTIVE SUMMARY . . . . .	ii
	ACKNOWLEDGMENT . . . . .	iv
	LIST OF SYMBOLS . . . . .	vii
	LIST OF TABLES . . . . .	x
	LIST OF FIGURES . . . . .	xi
1.0	INTRODUCTION . . . . .	1
2.0	MODELING OF PLUME DISPERSION . . . . .	3
	2.1 Physical Modeling of the Atmospheric Boundary Layer . . . . .	4
	2.1.1 Partial Simulation of the Atmospheric Boundary Layer . . . . .	5
	2.2 Physical Modeling of Plume Motion . . . . .	7
	2.2.1 Partial Simulation of Plume Motion . . . . .	9
	2.3 Modeling of Plume Dispersion at China Lake . . . . .	12
	2.3.1 Physical Modeling of the China Lake Atmospheric Surface Layer . . . . .	12
	2.3.2 Physical Modeling of the China Lake LNG Spill Plume . . . . .	13
3.0	DATA ACQUISITION AND ANALYSIS . . . . .	16
	3.1 Wind Tunnel Facilities . . . . .	16
	3.2 Model . . . . .	17
	3.3 Flow Visualization Techniques . . . . .	18
	3.4 Wind Profiles and Turbulence Measurements . . . . .	18
	3.5 Concentration Measurements . . . . .	20
	3.5.1 Hot Film Aspirating Probe . . . . .	20
	3.5.2 Errors in Concentration Measurement . . . . .	21
4.0	TEST PROGRAM RESULTS . . . . .	23
	4.1 Characteristics of the Approach Velocities . . . . .	24
	4.2 First Test Series Results . . . . .	24
	4.3 Second Test Series Results . . . . .	26
	4.4 Third Test Series Results . . . . .	26
	4.5 Fourth Test Series Results . . . . .	27
	4.6 Comparison with Field Data . . . . .	28



TABLE OF CONTENTS (continued)

<u>Chapter</u>	<u>Page</u>
REFERENCES . . . . .	33
TABLES . . . . .	36
FIGURES . . . . .	54
APPENDIX . . . . .	76

# LIST OF SYMBOLS

Dimensions are given in terms of mass (m), length, (L), time (t), moles (n), and temperature (T)

<u>Symbol</u>	<u>Definition</u>	
A	Area	$[L^2]$
$C_p$	Specific heat capacity at constant pressure	$[L^2 t^{-2} T^{-1}]$
D	Source diameter	$[L]$
g	Gravitational acceleration	$[L t^{-2}]$
k	Thermal conductivity	$[m L T^{-1} t^{-3}]$
L	Length	$[L]$
$\dot{m}$	Mass flow rate	$[m/t]$
M	Molecular weight	$[mn^{-1}]$
n	Mole	$[n]$
1/n	Exponent of velocity distributions power law	
p	Pressure	$[m L^{-1} t^{-2}]$
Q	Volumetric rate of gas flow	$[L^3 t^{-1}]$
T	Temperature	$[T]$
$\Delta T$	Temperature difference across some reference layer	$[T]$

# LIST OF SYMBOLS (continued)

<u>Symbol</u>	<u>Definition</u>	
t	Time	[t]
U	Velocity	[Lt <sup>-1</sup> ]
V	Volume	[L <sup>3</sup> ]
W	Plume vertical velocity	[Lt <sup>-1</sup> ]
x	General downwind coordinate	[L]
y	General lateral coordinate	[L]
z	General vertical coordinate	[L]
z <sub>0</sub>	Surface roughness parameter	[L]
δ	Boundary layer thickness	[L]
Λ	Integral length scale of turbulence	[L]
ν	Kinematic viscosity	[L <sup>2</sup> y <sup>-1</sup> ]
Δρ	Density difference between source gas and air	[ML <sup>-3</sup> ]
ρ	Density	[ML <sup>-3</sup> ]
σ	Standard deviation	
x	Mole fraction of gas component	
Ω	Angular velocity of earth = 0,726 x 10 <sup>-4</sup> (radians/sec)	[t <sup>-1</sup> ]
λ	Wave length	[L]

LIST OF SYMBOLS (continued)

Subscripts

a	Air
Ar	Argon
b.o.	Boiloff
g	Gas
i	Cartesian index
LNG	Liquified Natural Gas
m	Model
max	Maximum
NG	Natural gas
o	Reference conditions
p	Prototype
r	Reference
s	Source gas

# LIST OF TABLES

<u>Table</u>		<u>Page</u>
1	Summary of Concentration Tests . . . . .	36
2	Prototype Conditions . . . . .	37
3	Model Conditions . . . . .	38
4	Comparison of Similar LNG Tests at Different Model Scales . . . . .	39
5-1 to 5-5	Summary of Concentration Data . . . . .	40
6	Summary of Peak Concentration Data at Test Point Locations for Model and Field . . . . .	53

## LIST OF FIGURES

<u>Figure</u>	<u>Page</u>
1	Specific Gravity of LNG Vapor - Humid Atmosphere Mixtures . . . . . 54
2	Specific Gravity of Gas-Air Mixtures . . . . . 54
3	Variation of Froude Number for Gas-Air Mixtures . . . . . 55
4	Meteorological Wind Tunnel . . . . . 56
5	Environmental Wind Tunnel . . . . . 57
6	China Lake Test Site . . . . . 58
7	Field Concentration Measurement Locations . . . . 59
8	Model and Prototype Source Conditions for LNG-21 . 60
9	Velocity Probes and Velocity Standard . . . . . 61
10	Velocity Data Reduction Flow Chart . . . . . 62
11	Typical Response of Hot Film Aspirating Probe . . 63
12	Hot Film Aspirating Concentration Probe . . . . . 63
13	Velocity Profiles . . . . . 64
14	Local Longitudinal Turbulent Intensity Profile . . 64
15-1 to 15-8	Ground Contour Plot of Peak Concentration . . . . 65
16-1 to 16-2	Normalized Concentration Versus Downwind Distance . . . . . 73
17	Concentration Comparison for LLL Test 5 for LNG-21 . . . . . 75

## 1.0 INTRODUCTION

Natural gas is a highly desirable form of energy for consumption in the United States. Its conversion to heat energy for home and industrial use is achieved with very little environmental impact, and a sophisticated distribution network already services a major part of the country. Recent efforts to expand this nation's natural gas supply include the transport of natural gas in a liquid state from distant gas fields. Unfortunately storage and transport of liquid natural gas may include a relatively large environmental risk (Fay, 1973; Burgess, 1972). To transport and store liquified natural gas (LNG) it is cooled to a temperature of  $-162^{\circ}$  C. At this temperature if a storage tank on a ship or land were to rupture and the contents spill out onto the earth's surface, rapid boiling of the LNG would ensue and the liberation of a potentially flammable vapor would result. It is envisioned that if the flow from a rupture in a full LNG storage tank could not be constrained 28 million cubic meters of LNG would be released in 80 minutes (AGA, 1974). Past studies (Neff, 1976; AGA, 1974) have demonstrated that the cold LNG vapor plume will remain negatively buoyant for a majority of its lifetime; thus, it represents an extreme ground level hazard. This hazard will extend downwind until the atmosphere has diluted the LNG vapor below the lower flammability limit (a local concentration for methane below 5% by volume).

It is important that accurate predictive models for LNG vapor cloud physics be developed, so that the associated hazards of transportation and storage may be evaluated. Various industrial and governmental

agencies have sponsored a combination of analytical, empirical, and physical modeling studies to analyze problems associated with the transportation and storage of LNG. Since these models require assumptions to permit tractable solution procedure one must perform atmospheric scale tests to verify their accuracy.

The objectives of the present study were to help the Coast Guard and other contractors prepare for a series of atmospheric scale LNG spill tests at the China Lake Naval Weapons Center site and, subsequently to model the field program at reduced scales in meteorological wind tunnels. This test validation program was designed to examine the validity of physical modeling of an LNG vapor plume and to document any limitations of this technique.

The physical modeling study was conducted in two phases. The first phase was a pre-test series which provided general information that was needed in both the laboratory and field to set up instrumentation and investigate modeling techniques. The second phase was a post-test series in which four different spill tests were simulated in the wind tunnel. The meteorological and source conditions for these four tests are summarized in Table 1.

The methods employed in the physical modeling of atmospheric and plume motion are discussed in Chapter 2. The details of model construction and experimental measurements are described in Chapter 3. Chapter 4 discusses the test program and results obtained.



## 2.0 MODELING OF PLUME DISPERSION

To obtain a predictive model for a specific plume dispersion problem one must quantify the pertinent physical variables and parameters into a logical expression that determines their interrelationships. This task is achieved implicitly for processes occurring in the atmospheric boundary layer by the formulation of the equations of conservation of mass, momentum, and energy. These equations with site and source conditions and associated constitutive relations are highly descriptive of the actual physical interrelationship of the various independent (space and time) and dependent (velocity, temperature, pressure, density, etc.) variables.

These generalized conservation statements subject to the typical boundary conditions of atmospheric flow are too complex to be solved by present analytical or numerical techniques. It is also unlikely that one could create a physical model for which exact similarity exists for all the dependent variables over all the scales of motion present in the atmosphere. Thus, one must resort to various degrees of approximation to obtain a predictive model. At present purely analytical or numerical solutions of plume dispersion are unavailable because of the classical problem of turbulent closure (Hinze, 1975). Such techniques rely heavily upon empirical input from observed or physically modeled data. The combined empirical-analytical-numerical solutions have been combined into several different predictive approaches by Pasquill (1974) and others. The estimates of dispersion by these approaches are often crude; hence, they should only be used when the approach and site terrain are uniform and without obstacles. Boundary layer wind tunnels are

capable of physically modeling plume processes in the atmosphere under certain restrictions. These restrictions are discussed in the next few sections.

## 2.1 Physical Modeling of the Atmospheric Boundary Layer

The atmospheric boundary layer is that portion of the atmosphere extending from ground level to approximately 100 meters within which the major exchanges of mass, momentum, and heat occur. This region of the atmosphere is described mathematically by statements of conservation of mass, momentum, and energy (Cermak, 1971). The general requirements for laboratory-atmospheric-flow similarity may be obtained by fractional analysis of these governing equations (Kline, 1965). This methodology is accomplished by scaling the pertinent dependent and independent variables and then casting the equations into dimensionless form by dividing through by one of the coefficients (the inertial terms in this case). Performing these operations on such dimensional equations yields dimensionless parameters commonly known as:

Reynolds number	$Re = U_o L_o / \nu_o$	$= \frac{\text{Inertial Force}}{\text{Viscous Force}}$
Bulk Richardson number	$Ri = \left[ (\Delta T)_o / T_o \right] (L_o / U_o^2) g_o$	$= \frac{\text{Gravitational Force}}{\text{Inertial Force}}$
Rossby number	$Ro = U_o / L_o \Omega_o$	$= \frac{\text{Inertial Force}}{\text{Coriolis Force}}$
Prandtl number	$Pr = \nu_o / (k_o / \rho_o C_{p_o})$	$= \frac{\text{Viscous Diffusivity}}{\text{Thermal Diffusivity}}$
Eckert number	$Ec = U_o^2 / C_{p_o} (\Delta \bar{T})_o$	

For exact similarity between different flows which are described by the same set of equations, each of these dimensionless parameters must be equal for both flow systems. In addition to this requirement, there must be similarity between the surface-boundary conditions.

Surface-boundary condition similarity requires equivalence of the following features:

- a. Surface-roughness distributions,
- b. Topographic relief, and
- c. Surface-temperature distribution.

If all the foregoing requirements are met simultaneously, all atmospheric scales of motion ranging from micro to mesoscale could be simulated within the same flow field for a given set of boundary conditions (Cermak, 1975). However, all of the requirements cannot be satisfied simultaneously by existing laboratory facilities; thus, a partial or approximate simulation must be used. This limitation requires that atmospheric simulation for a particular wind-engineering application must be designed to simulate most accurately those scales of motion which are of greatest significance for the given application.

#### 2.1.1 Partial Simulation of the Atmospheric Boundary Layer

A partial simulation is practically realizable only because the kinematics and dynamics of flow systems above a certain minimum Reynolds number are independent of this number's magnitude (Schlichting, 1968; Zoric, 1972). The magnitude of the minimum Reynolds number will depend upon the geometry of the flow system being studied. Halitsky (1969) reported that for concentration measurements on a cube

placed in a near uniform flow field the Reynolds number required for invariance of the concentration distribution over the cube surface and downwind must exceed 11,000. Because of this invariance exact similarity of Reynolds parameter is neglected when physically modeling the atmosphere.

When the flow scale being modeled is small enough such that the turning of the mean wind directions with heights is unimportant, similarity of the Rossby number may be relaxed. For the case of dispersion of LNG near the ground level the Coriolis effect on the plume motion would be extremely small.

The Eckert number for air is equivalent to  $0.4 M_a^2 \left( \frac{T_o}{\Delta T_o} \right)$

where  $M_a$  is the mach number (Hinze, 1975). For the wind velocities and temperature differences which occur in either the atmosphere or the laboratory flow the Eckert number is very small; thus, the effects of energy dissipation with respect to the convection of energy is negligible for both model and prototype. Eckert number equality is relaxed.

Prandtl number equality is easily obtained since it is dependent on the molecular properties of the working fluid which is air for both model and prototype.

Bulk Richardson number equality may be obtained in special laboratory facilities such as the Meteorological Wind Tunnel at Colorado State University (Plate, 1963).

Quite often during the modeling of a specific flow phenomena it is sufficient to model only a portion of the boundary layer or a portion of the spectral energy distribution. This relaxation allows more flexibility in the choice of the length scale that is to be used in a model study. When this technique is employed it is common to scale the flow by any combination of the following length scales,  $\delta$ , the portion of the boundary layer to be simulated;  $z_0$ , the aerodynamic roughness;  $\Lambda_1$ , the integral length scale of the velocity fluctuations, or  $\lambda_p$ , the wave length at which the peak spectral energy is observed.

Unfortunately many of the scaling parameters and characteristic profiles are difficult to obtain in the atmosphere. They are infrequently known for many of the sites to which a model study is to be performed. To help alleviate this problem Counihan (1975) has summarized measured values of some of these different descriptions for the atmospheric flow at many different sites and flow conditions.

## 2.2 Physical Modeling of Plume Motion

In addition to modeling the turbulent structure of the atmosphere in the vicinity of a test site it is necessary to properly scale the plume source conditions. One approach would be to follow the methodology used in Section 2.1., i.e., writing the conservation statements for the combined flow system followed by fractional analysis to find the governing parameters. An alternative approach, the one which will be used here, is that of similitude (Kline, 1965). The method of similitude obtains scaling parameters by reasoning that the mass ratios, force ratios, energy ratios, and property ratios should be equal for both model and prototype. When one considers the dynamics of gaseous

plume behavior the following nondimensional parameters of importance are identified (Hoot, 1974; Skinner, 1978; Snyder, 1972; Halitsky, 1969).<sup>1,2</sup>

$$\begin{aligned}\text{Mass Ratio} &= \frac{\text{mass flow of plume}}{\text{effective mass flow of air}} \\ &= \frac{\rho_s W_s A_s}{\rho_a U_a A_a} = \frac{\rho_s Q}{\rho_a U_a L^2}\end{aligned}$$

$$\begin{aligned}\text{Momentum Ratio} &= \frac{\text{inertia of plume}}{\text{effective inertia of air}} \\ &= \frac{\rho_s W_s^2 A_s}{\rho_a U_a^2 A_a} = \frac{\rho_s Q^2}{\rho_a U_a^2 L^4}\end{aligned}$$

$$\begin{aligned}\text{Densimetric Froude No. (Fr)} &= \frac{\text{effective inertia of air}}{\text{buoyancy of plume}} \\ &= \frac{\rho_a U_a^2 A_a}{g(\rho_g - \rho_a) V_s} = \frac{U_a^2}{g(\frac{\rho_s - \rho_a}{\rho_a}) L}\end{aligned}$$

$$\begin{aligned}\text{Volume Flux Ratio} &= \frac{\text{Volume flow of plume}}{\text{effective volume flow of air}} \\ &= \frac{Q}{U L^2}\end{aligned}$$

to obtain simultaneous simulation of these four parameters it is necessary to maintain equality of the plume's specific gravity

$$\rho_s / \rho_a.$$

<sup>1</sup>It has been assumed that the dominant transfer mechanism is that of turbulent entrainment. Thus the transfer processes of heat conduction, convection, and radiation are negligible.

<sup>2</sup>The scaling of plume Reynolds number is also a significant parameter. Its effects are invariant over a large range thus making it possible to scale the distribution of mean and turbulent velocities and relax exact parameter equality.

### 2.2.1 Partial Simulation of Plume Motion

The restriction to an exact variation of the density ratio for the entire life of a plume is difficult to meet for plumes which simultaneously vary in molecular weight and temperature. To emphasize this point more clearly, consider the mixing of two volumes of gas, one being the source gas,  $\psi_s$ , the other being ambient air,  $\psi_a$ . Consideration of the conservation of mass and energy for this system yields (Skinner, 1978):<sup>1</sup>

$$\frac{\rho_g}{\rho_a} = \frac{\frac{\rho_s}{\rho_a} \psi_s + \psi_a}{\left( \frac{T_a}{T_s} \psi_s + \psi_a \right) \left( \frac{C_{p_s} M_s}{C_{p_a} M_a} \psi_s + \psi_a \right) / \left( \frac{C_{p_s} M_s}{C_{p_a} M_a} \frac{T_a}{T_s} \psi_s + \psi_a \right)} \quad (2-7)$$

If the temperature of the air,  $T_a$ , equals the temperature of the source gases,  $T_s$ , or if the product,  $C_p M$ , is equal for both source gas and air then the equation reduces to:

$$\frac{\rho_g}{\rho_a} = \frac{\frac{\rho_s}{\rho_a} \psi_s + \psi_a}{\psi_s + \psi_a} \quad (2-8)$$

Thus for two prototype cases: 1) an isothermal plume and 2) a thermal plume which is composed of air, it does not matter how one models the density ratio as long as the initial density ratio value is equal for both model and prototype.

<sup>1</sup>The pertinent assumption in this derivation is that the gases are ideal and properties are constant.

For a plume whose temperature, molecular weight, and specific heat are all different from that of the ambient air, i.e., a cold natural gas plume, equality in the variation of the density ratio upon mixing must be relaxed slightly if one is to model utilizing a gas different from that of the prototype.<sup>1</sup> In most situations this deviation from exact similarity is very small. (See discussion Section 3.2 and Figure 2.)

Scaling of the effects of heat transfer by conduction, convection, radiation, or latent heat release from entrained water vapor cannot be reproduced when the model source gas and environment are isothermal. Fortunately in a large majority of industrial plumes the effects of heat transfer by conduction, convection, and radiation from the environment are small enough that the plume buoyancy essentially remains unchanged. The influence of latent heat release by moisture upon the plume's buoyancy is a function of the quantity of water vapor present in the plume and the humidity of the ambient atmosphere. Such phase change effects on plume buoyancy can be very pronounced in some prototype situations. Figure 1 displays the variation of specific gravity from a spill of liquified natural gas in atmospheres of different humidities.

A reasonably complete simulation may be obtained in some situations even when modified density ratio  $\rho_s/\rho_a$  is stipulated. The advantage of such a procedure is demonstrated most clearly by the statement of equality of Froude numbers.

---

<sup>1</sup>If one was to use a gas whose temperature is different from that of the ambient air then consideration of similarity in the scaling of the energy ratios must be considered.



$$\left( \frac{U_a^2}{\left( \frac{\rho_s}{\rho_a} - 1 \right) Lg} \right)_m = \left( \frac{U_a^2}{\left( \frac{\rho_s}{\rho_a} - 1 \right) Lg} \right)_p$$

Solving this equation to find the relationship between model velocity and prototype velocity yields:

$$(U_a)_m = \left( \frac{S.G._m - 1}{S.G._p - 1} \right)^{\frac{1}{2}} \left( \frac{L_p}{L_m} \right)^{\frac{1}{2}} (U_a)_p$$

where S.G. is the specific gravity,  $(\rho_s/\rho_a)$ , and L.S. is the length scale,  $(L_p/L_m)$ . By increasing the specific gravity of the model gas compared to that of the prototype gas, for a given length scale, one increases the reference velocity used in the model. It is difficult to generate a flow which is similar to that of the atmospheric boundary layer in a wind tunnel run at very low wind speeds. Thus the effect of modifying the models specific gravity extends the range of flow situations which can be modeled accurately. But unfortunately during such adjustment of the model gas's specific gravity at least two of the four similarity parameters listed must be neglected. The options as to which two of these parameters to retain, if any, depends upon the physical situation being modeled. Two of the three possible options are listed below.

- (1) Froude No. Equality  
 Momentum Ratio Equality  
 Mass Ratio Inequality  
 Velocity Ratio Inequality<sup>1</sup>

<sup>1</sup>When this technique is employed distortion in velocity scales or similarly volume flow rates requires a correction in source strength.

- (2) Froude No. Equality
- Momentum Ratio Inequality
- Mass Ratio Inequality
- Velocity Ratio Equality

Both of these schemes have been used to model plume dispersion downwind of an electric power plant complex (Skinner, 1978) and (Meroney, 1974) respectively.

The modeling of the plume Reynolds number is relaxed in all physical model studies. This parameter is thought to be of small importance since the plume's character will be dominated by background atmospheric turbulence soon after its emission. But, if one was interested in plume behavior near the source, then steps should be taken to assure that the model's plume is fully turbulent.

### 2.3 Modeling of Plume Dispersion at China Lake

In the sections above a review of the extent to which wind tunnels can model plume dispersion in the atmospheric boundary layer has been presented. In this section these arguments will be applied to the specific case of an LNG spill at the China Lake Naval Weapons Center.

#### 2.3.1 Physical Modeling of the China Lake Atmospheric Surface Layer

Only small quantities of LNG are being spilt at the China Lake test site, approximately five cubic meters; hence, it was decided to scale the topography at the site by a one-to-eightyfive ratio to improve the resolution during concentration measurements. At this scale it is not possible to simulate the entire depth of the atmospheric boundary layer. This lack of simulation of the entire boundary layer is considered to be of minor consequence since the source is at the ground level

and the vertical dispersion in the near field is minimal. The aerodynamic roughness ( $z_0$ ), power exponent ( $1/n$ ), and the integral length scales of turbulence  $\Lambda_i$  were all scaled to prototype equivalent values at a two meter height. The specific values obtained are listed in Table 6. A preliminary validation program was conducted at a model scale of 1:170 to assure that this partial depth simulation method yielded reasonably consistent results over two different scale ratios.

The equality of Richardson numbers was not specified. During tests simulated herein the prevailing prototype conditions were either neutral or only slightly unstable; thus, buoyancy generated turbulence played only a small role in determining ground level turbulent structure.

#### 2.3.2 Physical Modeling of the China Lake LNG Spill Plume

The buoyancy of a plume resulting from an LNG spill is a function of both the mole fraction of methane and temperature. If the plume entrains air adiabatically, then the plume would remain negatively buoyant for its entire lifetime. If the humidity of the atmosphere were high then the state of buoyancy of the plume will vary from negative to weakly positive. These conclusions are born out in Figure 1, which illustrates the specific gravity of a mixture of methane at boiloff temperature with ambient air and water vapor.

Since the adiabatic plume assumption will yield the most conservative downwind dispersion estimates this situation was simulated. Several investigators have confirmed that the Froude number is the parameter which governs plume spread rate, trajectory, plume size and entrainment during initial dense plume dilution (Hoot and Meroney, 1974; Bodurtha,

1961; Van Ulden, 1974; Boyle and Kneebone, 1973). The modeling of momentum is not of critical importance for a ground source released over a fairly large area. The equality of model and prototype specific gravity was relaxed so that pure Argon gas could be used for the model source gas.

Argon provides almost eight times the detection sensitivity for instantaneous concentration measurements as the carbon dioxide used in previous studies (Meroney, 1977). The variation of specific gravity with equivalent observed mole fraction of methane for these different gases is plotted in Figure 2. The variation of Froude number with equivalent mole fraction of methane for the simulation gas used, Argon, is plotted in Figure 3. Over the concentration range where the buoyancy forces are dominant the variation of the Froude number is properly simulated. Undistorted scaling of velocity components was maintained, which implies the undistorted scaling of source strength.

The actual source condition, boiloff rate per unit area over the time duration of the spill, for a spill of LNG on water is highly unpredictable. As there was no data on the variable area and variable volume nature of the different LNG tests conducted at China Lake the source conditions were approximated by assuming a steady boiloff rate for the duration of the spill over a constant area.

Since the thermally variable prototype gas was simulated by an isothermal simulation gas, the concentration measurements observed in the model must be adjusted to equivalent concentrations that would be measured in the field. This relationship which is derived in Appendix A is:

$$x_p = \frac{x_m}{x_m + (1 - x_m) \frac{T_s}{T_a}}$$

where

$x_m$  = volume or mole fraction measured during the model tests

$T_s$  = source temperature of LNG during field conditions

and  $T_a$  = ambient air temperature during field conditions

### 3.0 DATA ACQUISITION AND ANALYSIS

The methods used to make laboratory measurements and the techniques used to convert these measured quantities to meaningful field equivalent quantities are discussed in this section. Attention has been drawn to the limitations in the techniques in an attempt to prevent misinterpretation or misunderstanding of the results presented in the next section. Some of the methods used are conventional and need little elaboration.

#### 3.1 Wind Tunnel Facilities

The first test series of the experiments were performed in the Meteorological Wind Tunnel (MWT) shown in Figure 4. This wind tunnel, especially designed to study atmospheric flow phenomena, incorporates special features such as an adjustable ceiling, temperature controlled boundary walls, and a long test section to permit reproduction of micrometeorological behavior. Mean wind speeds of 0.3 to 40 m/s can be obtained in the MWT. Boundary-layer thickness up to 1.2 m can be developed "naturally" over the downstream 6 m of the MWT test section. Thermal stratification in the MWT is provided by the heating and cooling systems in the section passage and test section floor. The flexible test section roof on the MWT is adjustable in height to permit the longitudinal pressure gradient to be set at zero. The MWT facility is described in detail by Plate and Cermak (1963).

A set of vortex generators was installed 0.6 m downwind of the entrance to give the simulated boundary layer an initial impulse of growth. These vortex generators were then followed by 9 m of smooth floor and a 3 m approach ramp to the 1:170 scaled topography of the China Lake site.

The Environmental Wind Tunnel (EWT) shown in Figure 5 was used for the remaining three test series. This wind tunnel, specially designed to study atmospheric flow phenomena, incorporates special features such as adjustable ceiling, rotating turntables, transparent boundary walls, and a long test section to permit reproduction of micrometeorological behavior at larger scales. Mean wind speeds of 0.15 to 12 m/s can be obtained in the EWT. Boundary layer depths 1 m thick over the downstream 6 meters can be obtained with the use of the vortex generators at the test section entrance and surface roughness on the floor. The flexible test section roof on the EWT is adjustable in height to permit the longitudinal pressure gradient to be set at zero. The vortex generators at the tunnel's entrance were followed by 10 m of smooth floor, and a 3 m approach ramp to the 1:85 scaled topography at the China Lake site.

### 3.2 Model

A 1:170 scale model of the China Lake topography was constructed for use in the Meteorological Wind Tunnel and a 1:85 scale model was constructed for use in the Environmental Wind Tunnel. The topographic relief of the China Lake site is shown in Figure 6. Both these models were constructed of 0.64 cm thick styrofoam sheets. A cylindrical plenum manufactured with perforated upper plate was centered in the middle of the test site pond. The source gas, Argon, stored in a high pressure cylinder was directed through a solenoid valve, a flow meter, and onto the circular area source mounted in the model pond. Typical curves of the boiloff duration and source diameter are shown in Figure 7.

All source release conditons were step functions; thus, their profiles can be recreated from the data in Table 3.

### 3.3 Flow Visualization Techniques

Smoke was used to define plume behavior over the China Lake site. The smoke was produced by passing the simulation gas, Argon, through a container of titanium tetrachloride located outside the wind tunnel. The plume was illuminated with arc-lamp beams. A visible record was obtained by means of pictures taken with a Speed Graphic camera utilizing Polaroid film for immediate examination. Additional still pictures were obtained with a 35 mm camera. The color motion pictures were taken with a Bolex motion picture camera.

### 3.4 Wind Profiles and Turbulence Measurements

Velocity profile measurements and reference wind speed conditions were obtained with a Thermo-Systems Inc. (TSI) 1050 anemometer and a TSI model 1210 hot film probe. Turbulence measurements were made with this system for the longitudinal velocity component and with a TSI split film probe connected to two TSI 1050 anemometers for both longitudinal and vertical component measurements. Since the voltage response of these anemometers is non-linear with respect to velocity, a multi-point calibration of system response versus velocity was utilized for data reduction.

The velocity standard utilized in the present study was that depicted in Figure 8. This consisted of a Matheson model 8116-0154 mass flowmeter, a Yellow Springs thermistor, and a profile conditioning section constructed by the Engineering Research Center shop. The mass



flowmeter measures mass flow rate independent of temperature and pressure, the thermistor measures the temperature at the exit conditions, and the profile conditioning section forms a flat velocity profile of very low turbulence at the position where the probe is to be located. Incorporating a measurement of the ambient atmospheric pressure and a profile correction factor permits the calibration of velocity at the measurement station from 0.0-2.0 m/s  $\pm$  5.0 cm/s.

During calibration of the single film anemometer, the anemometer voltage response values over the velocity range of interest were fit to an expression similar to that of King's law (Sandborn, 1972) but with a variable exponent determined by least squares method. The accuracy of this technique is approximately  $\pm$  2 percent of the actual longitudinal velocity.

The split film probe was mounted on a rotatable mechanism with a precision protractor accurate to  $\pm$  2 minutes and positioned in front of the velocity standard. The calibration procedure is described in the TSI Technical Bulletin 20. The suggested calibration equations were fit to the data by a least squares method. The accuracy of this technique is approximately  $\pm$  5 percent of the actual longitudinal or vertical velocity values.

The velocity sensors were mounted on a vertical traverse and positioned over the measurement location on the model. The anemometer's responses were fed to a Preston analog-to-digital converter and then directly to a HP-1000 minicomputer for immediate interpretation. The HP-1000 computer also controls probe position. A flow chart depicting the control sequence for this process is presented in Figure 9.

### 3.5 Concentration Measurements

The concentrations of methane produced during an LNG spill are inherently time dependent. It is necessary to have a frequency response to concentration fluctuations of at least 50 Hz to isolate peaks of methane concentrations above 5 percent (the lower flammability limit of methane in air, LFL); hence, an aspirating hot film probe was used for this study.

#### 3.5.1 Hot Film Aspirating Probe

The basic principles governing the behavior of such a probe have been discussed by Blackshear and Fingerson (1962), Brown and Rebollo (1972), and Kuretsky (1967). A diagram of the design of this probe is presented in Figure 11. A vacuum source sufficient to choke the flow through the small orifice just downwind of the sensing elements was applied. Only one of the two films in this special probe was an active element for the measurement of concentration in the present study. This film was operated in a constant temperature mode at a temperature above that of the ambient air temperature. A feedback amplifier maintained a constant overheat resistance through adjustment of the heating current. A change in output voltage from this sensor circuit corresponds to a change in heat transfer between the hot-wire and the sampling environment.

The heat transfer rate from a hot cylindrical film to a gas flowing over it depends primarily upon the film diameter, the temperature difference between the film and the gas, the thermal conductivity and viscosity of the gas, and the gas velocity. For a film in an aspirated probe with a sonic throat, the gas velocity can be expressed as a function of the ratio

of the probe cross-sectional area at the film position to the area at the throat, the specific heat ratio, and the speed of sound in the gas. The latter two parameters, as well as the thermal conductivity and viscosity of the gas mentioned earlier, are determined by the gas composition and temperature. Hence, for a fixed probe geometry and film temperature, the heat transfer rate, or the related voltage drop across the film is a function of only the gas composition and temperature. Since all tests performed in this study were in an isothermal flow situation the film's response was only a function of gas composition.

During probe calibration known compositions of Argon-air mixtures were passed through a pre-heat exchanger to condition the gas to the tunnel temperature environment. These known compositions were produced from a bottle of pure Argon and bottle of pure air passed through a Matheson gas proportioner or drawn from a bottle of prepared gas composition provided by Matheson Laboratories. Figure 10 displays the measured variation of the voltage drop with percentage of Argon in an Argon-air mixture for three different values of the film temperature overheat. For an overheat ratio (temperature of film/ambient temperature) of 1.75 the voltage drop varies linearly with Argon concentration and has the maximum sensitivity. This particular overheat ratio was used during all wind tunnel measurements.

### 3.5.2 Errors in Concentration Measurement

The effective sampling area of the probe inlet is a function of the probe's aspiration rate and the distribution of approach velocities of the gases to be sampled. A calculation of the effective sampling area during all tests suggests that the effective sampling area was

always less than the area of the probe's inlet,  $1.88 \text{ cm}^2$ . Thus the resolution of the concentration measurements as applied to the China Lake site is  $\sim 1.6 \text{ m}^2$ .

The travel time from the sensor to the sonic choke limits the upper frequency response of the probe. At high frequencies the correlation between concentration fluctuation and velocity fluctuations (velocity fluctuations are a result of the changes of sonic velocity with concentration) at the sensor begin to decline. The CSU aspirated probe is expected to have a 1000 Hz upper frequency response, but, to improve signal to noise characteristics, the signal was filtered at 200 Hz. This is well above the frequencies of concentration fluctuations that were expected to occur.

The errors caused by a linearity assumption in the reduction of concentration data are approximately the component value (percent Argon)  $\pm 0.75$  percent. The errors caused by calibration change due to temperature drift are approximately 0.1 percent of the component value per degree centigrade. Since the tunnel temperatures vary at most  $\pm 5^\circ\text{C}$  during a given test period the maximum error due to temperature drift would be 0.5 percent of the component value.

#### 4.0 TEST PROGRAM RESULTS

The test program consisted of four different test series. The first test series objectives were:

- To determine the general behavior of LNG spills at the China Lake facility.
- To obtain concentrations and photographs of the behavior of these tests scaled at 1:170 to compare with tests performed at a scale of 1:85 as a measure of the quality of the simulation criteria.
- To examine the scaling implications of adjusting the initial specific gravity of the model to be different from that of the prototype.

The second test series objectives were:

- To determine the general behavior of LNG spills at the China Lake facility.
- To obtain concentrations and photographs of the behavior of these tests scaled at 1:85 to compare to the 1:170 scales test performed earlier.

The third test series objectives were:

- To obtain concentration data for the field tests, LNG-18 and LNG-19 at a scale of 1:85 in the presence of the China Lake topography and with a smooth floor.
- To obtain spectral measurements of longitudinal and vertical velocity components at two different sites on the China Lake model.

The fourth test series objectives were:

- To simulate the field tests, LNG-18, 19, 20, and 21 and obtain concentration measurement of these tests over the 1:85 scale model of China Lake.

A summary of all tests simulated in the laboratory is presented to Table 1. A detailed summary of the prototype and model test conditions for LNG-18, 19, 20, and 21 is presented in Tables 2 and 3 respectively. All dimensions reported in the following sections have been converted to equivalent full-scale values appropriate to the China Lake site. The origin is referenced as the LNG spill point. The positive x-axis is in the direction of the prevailing wind for all coordinate systems unless otherwise mentioned.

#### 4.1 Characteristics of the Approach Velocities

Measurements of the approach flow characteristics were obtained for the modeled flow over the China Lake scale topography. As discussed in Section 2.1.1 these characteristic length and velocity scales should be comparable to those expected to occur over the China Lake site. Counihan (1975) has summarized the values of aerodynamic roughness,  $z_0$ , longitudinal velocity integral length scale,  $\Lambda_x$ , and the power law index,  $1/n$ , that may be expected to occur in the atmosphere. Table 6 compares values of these quantities as cited by Counihan and values scaled up from the model tests. Figures 13 and 14 show the profiles of mean velocity and local turbulent intensity respectively.

#### 4.2 First Test Series Results

A 1:170 scale model of the China Lake site was placed in the Meteorological Wind Tunnel facility (MWT). Five different tests were performed on the model. Each was performed with a spill volume of 5.95 cubic meters of LNG and a boiloff rate of 33.6 kg/s. Two different wind directions and three different wind speeds were considered. These conditions

are summarized in Table 3. Black-and-white Polaroid photographs were taken of the different spill conditions so that plume configurations could be compared to tests performed over the 1:85 scale model. Time dependent concentration measurements were obtained at three axial distances downwind for each test. Table 5-1 summarizes the times of arrival, peak concentrations, time for passage of the plume and value of peak concentration for the various measurements sites.

Visualization of the lowest wind speed simulated, 2.2 m/s, indicated an unexpectedly large vertical dispersion rate. The concentration measurements confirmed this observation. It was concluded that this abnormal vertical variance was associated with instabilities in the MWT while operating below a minimum stable operational wind speed.

Tests were also performed to test the advisability of relaxing precise equality of the density, mass, and momentum ratios discussed in the simulation chapter (see Section 2.2 and 2.3). Argon gas (specific gravity of 1.38), carbon dioxide gas (specific gravity of 1.52), and compressed air (specific gravity of 1.00) were used as source gases released from an area source on a smooth floor. Wind speeds were low enough so that pronounced gravity spreading was exhibited. From these tests in which both visual plume pattern and concentration measurements were obtained it was concluded that very similar behavior was exhibited by both simulation schemes. A  $\pm 15\%$  variation in source Froude number was not detectable in the resultant plume.

#### 4.3 Second Test Series Results

A 1:85 scale model of the China Lake site was placed in the Environmental Wind Tunnel facility (EWT). Four different tests were performed on the model. The transient boiloff experiments were adjusted to simulate a spill volume of 5.95 cubic meters of LNG. Steady state boiloff experiments were run at a continuous boiloff rate of 33.6 kg/s. The time duration of the boiloff was for practical purposes infinite. Three different wind speeds were tested approaching from the southwest. These conditions are summarized in Table 3. Black-and-white Polaroid photographs and color slides were obtained for the steady boiloff releases and a 16 mm color movie was prepared for all tests. Table 5-2 and 5-3 summarize the time of arrival, peak concentrations, time for passage of the plume and the value of peak concentrations.

Measurements from the first test series in the MWT on a 1:170 scale model and measurements from this test series on a 1:85 scale model may be compared. Inspecting Table 4, it can be concluded that concentrations measured at different model scales are generally of the same order except for the cases in which the MWT tunnel was run at its lowest speed. It was mentioned in Section 4.2 that this speed was felt to be below the operational limit of the MWT. Since the number of measurement locations and test replications were very limited in the MWT no conclusions can be made concerning the quantitative influence of model scale on the simulation.

#### 4.4 Third Test Series Results

The China Lake boiloff rate, boiloff duration, and wind speed of the LNG-18 and LNG-19 tests were simulated in the Environmental Wind Tunnel with a smooth floor. The same tests were then repeated, but this time



the topography of the China Lake site was included.<sup>1</sup> Thorough concentration measurements downwind of these four tests were obtained. A summary of the test conditions for these four tests is presented in Table 3. Approximate hand drawn ground level peak concentration contours are shown in Figures 15-1 through 15-4 for all four tests. The maximum normalized concentration coefficient versus downwind distances for the two tests without the topography is presented in Figure 16-1. A summary of the times of arrival, peak concentration and passage of the plume and the maximum peak concentration observed is presented in Table 5-4.

It is seen from a comparison of the similar tests one performed with topography and one performed on a smooth floor, that the dispersion at the China Lake site is greater than what would be experienced if the spill occurred in a very smooth and flat area.

Spectral measurements of the longitudinal and vertical velocity fluctuations were obtained at two different locations at a height of 2 m over the China Lake scaled topography. A discussion of these measurements appears in Section 4.1 on the simulated characteristics of wind motion over the China Lake site.

#### 4.5 Fourth Test Series Results

A 1:85 scale model of the China Lake site was placed in the Environmental Wind Tunnel. Concentration measurements were obtained downwind of the simulated field tests LNG-18, LNG-19, LNG-20, and LNG-21. A summary of the field conditions that were simulated is presented in Table 1. A summary of the model conditions for these tests is presented

<sup>1</sup>Unfortunately the wind directions provided by the field investigators were in error. These two tests were rerun in the fourth test series.

in Table 2. Ground level peak concentration contours are shown in Figures 15-5 through 15-8 for each test. The maximum normalized concentration versus downwind distance for all four tests are shown in Figure 16-2. A summary of the time of arrival, peak concentration and passage of the plume and the maximum peak concentration observed is presented in Table 5-5.

#### 4.6 Comparison with Field Data

As part of the current China Lake test series, field concentration measurements were obtained over two independent measurement grids. The Naval Weapons Test Center established a grid of ten different concentration measurement stations and the Lawrence Livermore Laboratory (LLL) provided eight towers with a variety of concentration sampling equipment. The primary purpose of the LLL grid was sensor evaluation. Both these grids are described on Figure 7.

The degree to which physically modeled data correlates to values which are obtained in the field is dependent upon the approximations which were assumed in the formulation of the model and the inherent randomness of the atmospheric diffusion processes. The assumptions employed in the construction of a physical model of LNG vapor dispersion at the Naval Weapons Test Center are discussed in Section 2.3. The randomness of wind directions and velocities in the atmosphere are such that a single time realization of a fixed point in space is insufficient to describe the complete probability distribution of peak concentrations that may be observed at that point. Without ensemble averaging of similar tests in the field the values found during a single realization

may range over a better portion of an unknown probability distribution. Pasquill (1974) notes that in many circumstances of practical interest the uncertainties found between continuous releases of gaseous plumes may at best be ten to fifty percent in the average and factors of two or more individually. In addition to the small scale effects of local randomness, the atmosphere has large scale effects which lead to meandering of plume mean motion. These large scale meanderings are not modeled in wind tunnels.

The Naval Weapons Test Center grid consisted of ten different concentration sensors. These instruments were all of the catalytic combustion type. The principle of operation of these instruments is that a hot catalytic filament causes the methane to oxidize, and the rise in temperature due to the reaction changes the electrical resistance of the filament. These detectors are accurate for only low (below 7%), slowly varying methane concentration.

Table 7 compares peak concentrations observed in the field at the Naval Weapons test grid points with those obtained over a physical model. This comparison is in general quite poor. There are several factors which may account for this scatter in comparable data over several orders of magnitude. That are: (1) the mean wind direction specified for each wind-tunnel test may have been in error; (2) the fluctuations present during the field tests were as large as  $\pm 50^\circ$  (physical modeling of large wind direction fluctuations is not possible in a wind tunnel); (3) the wind speed observed in the field changed by as much as  $\pm 1.8$  m/s during the tests (this amount of fluctuation can account for approximately  $\pm 50\%$  variation in concentration

values); (4) the peak concentration fluctuations in the field tests were too rapid for the catalytic sensor to respond; (5) the concentrations were too large for the catalytic sensors to respond; (6) the approximations used in simulating the LNG field test series were too weak to achieve proper simulation.

The Lawrence Livermore Laboratory obtained concentration time histories at a variety of different heights on their eight towers equipped with concentration sensors. Several different types of sensors were employed. Each of these detector responses was verified by simultaneous grab bag sampling of the gases flowing over the sensor. This technique provides an accurate method of verifying the different sensors' response were correct. The peak field concentration obtained from the lowest sensor elevation at each of the eight towers is summarized along with approximate model values in Table 7. Since concentrations over the model were not obtained at the Lawrence Livermore grid sites, the values noted for model equivalents are only approximate. These values were obtained by interpolation of the hand drawn ground level peak concentration contours in Figures 15-15 through 15-8. On these figures the circled numbers are the peak concentrations observed in the field on the Lawrence Livermore grid. Figure 17 displays the time variation of LNG vapor concentration for both modeled and field data at LLL grid point 5 for the test spill LNG-21.

The correlation between Lawrence Livermore data and that of the model data is generally superior to that found between the Naval Weapons Test Center data and that of the model. There remain, however, a number of sampling points where poor agreement exists. Considering each test point at a time for LNG-18 shows reasonable comparison, within a 50% of the field value, for the near field grid points 1, 2, and 3, and poor comparison on grid point four. The reason for these discontinuities in field-model comparisons may be any combination of the factors mentioned previously. In this case the differences appear to be caused by the small number of measurement locations in both field and model tests and the variability of wind direction in the field. For LNG-19 the quality of comparison between model and field data is somewhat poor. The decay of concentration with distance from the source appears to agree, but the direction of the plume appears to be different. This result suggests a change in wind direction between field data and what was modeled. Here again as in LNG-18 an insufficient number of model or field measurement locations were taken to define the concentration field properly. In LNG-20 the comparison between field and model again appears to be poor. The laboratory model predicts that at this higher wind speed (12.4 m/s at 2 m) the LNG plume has very little lateral spread, but the field measurement show concentrations at large distances from the plume's mean axis. This suggests a large variation in wind direction or an error in the mean wind direction. For this test and the LNG-21 a sufficient number of measurement locations were used to define the model ground level contours properly, 47 and 91 points respectively. LNG-21 shows the best comparison between model and

field results for the four tests modeled. Each measurement location has an acceptable comparison considering the field variation of wind direction and velocity and that there are insufficient field data points to define ground level peak concentration patterns.

## REFERENCES

- American Gas Association (1974) "LNG Safety Program, Interim Report on Phase II Work," Report on American Gas Association Project IS-3-1, Battelle Columbus Laboratories.
- Blackshear, P. L., Jr., and Fingerson, L. (1962) "Rapid Response Heat Flux Probe for High Temperature Gases," ARS Journal, November 1962, pp. 1709-1715.
- Bodurtha, F. T., Jr. (1961) "The Behavior of Dense Stack Gases," J. of APCA, Vol. 11, No. 9, pp. 431-437.
- Boyle, G. J. and Kneebone, A. (1973) "Laboratory Investigation Into the Characteristics of LNG Spills on Water, Evaporation, Spreading and Vapor Dispersion," Shell Research, Ltd., Report to API, March.
- Brown, G. L. and Rebollo, M. R. (1972) "A Small, Fast Response Probe to Measure Composition of a Binary Gas Mixture," AIAA Journal, Vol. 10, No. 5, pp. 649-752.
- Burgess, D. S., Biardi, J., and Murphy, J. N. (1972) "Hazards of Spillage of LNG Into Water," Bureau of Mines, MIPR No. Z-70099-9-12395.
- Cermak, J. E. (1971) "Laboratory Simulation of the Atmospheric Boundary Layer," AIAA J1., Vol. 9, No. 9, pp. 1746-1754, September.
- Cermak, J. E. (1975) "Applications of Fluid Mechanics to Wind Engineering, A Freeman Scholar Lecture," J. of Fluid Engineering, Vol. 97, Ser. 1, No. 1, pp. 9-38.
- Counihan, J. (1975) "Adiabatic Atmospheric Boundary Layers: A Review and Analysis of Data From the Period 1880-1972," Atmospheric Environment, Vol. 9, pp. 871-905.
- Davies, P. O. A. L., and Moore, P. L. (1964) "Experiments on the Behavior of Effluent Emitted From Stacks at or Near the Roof Level of Tall Reactor Buildings," Int. Journal of Air Water Pollution, Vol. 8, pp. 515-533.
- Davenport, A. G. (1963) "The Relationship of Wind Structure to Wind Loading" Proceedings of Conference on Buildings and Structures, National Physical Laboratory, Great Britain, pp. 54-83.
- Fay, J. A. (1973) "Unusual Fire Hazard of LNG Tanker Spills," Combustion Science and Technology, Vol. 7, pp. 47-49.

- Halitsky, J. (1969) "Validation of Scaling Procedures for Wind Tunnel Model Testing of Diffusion Near Buildings," Geophysical Sciences Laboratory, Report No. TR-69-8, New York University, New York.
- Hinze, J. O. (1975) Turbulence, McGraw-Hill, 790 pp.
- Hoot, T. G. and Meroney, R. N. (1974) "The Behavior of Negatively Buoyant Stack Gases," 67th Annual Meeting APCA, June 9-13, 1973, Denver, Colorado, Paper No. 74-210, 21 pp.
- Kaimal, J. C., Wyngaard, J. C., Izumi, T., and Coté, O. R. (1972) "Spectral Characteristics of Surface-Layer Turbulence" Quarterly Journal of the Royal Meteorological Society, Vol. 98, pp. 563-589.
- Kline, S. J. (1965) Similitude and Approximation Theory, McGraw-Hill, 229 pp.
- Kuretsky, W. H. (1967) "On the Use of an Aspirating Hot-Film Anemometer for the Instantaneous Measurement of Temperature," Thesis, Master of Mechanical Engineering, University of Minnesota, Minneapolis.
- Meroney, R. N., et al. (1974) "Wind Tunnel Study of Stack Gas Dispersal at the Avon Lake Power Plant," Fluid Dynamics and Diffusion Laboratory Report CER73-74RNM-JEC-BTY-SKN35. Colorado State University, Fort Collins, Colorado, April.
- Meroney, R. N., Neff, D. E., Cermak, J. E., and Megahed, M. (1977) "Dispersion of Vapor From LNG Spills - Simulation in a Meteorological Wind Tunnel," Report Prepared for R & D Associates, California, Fluid Dynamics and Diffusion Laboratory Report CER76-77RNM-JEC-DEN-MM57, Colorado State University, Fort Collins, Colorado, 151 pp.
- Neff, D. E., Meroney, R. N., and Cermak, J. E. (1976), "Wind Tunnel Study of Negatively Buoyant Plume Due to an LNG Spill," Report Prepared for R & D Associates, California, Fluid Dynamics and Diffusion Laboratory Report CER76-77DEN-RNM-JEC22, Colorado State University, Fort Collins, Colorado, 241 pp.
- Pasquill, F. (1974) Atmospheric Diffusion, D. von Nostrand Co., 429 pp.
- Plate, E. J. and Cermak, J. E. (1963) Micro-Meteorological Wind-Tunnel Facility: Description and Characteristics," Fluid Dynamics and Diffusion Laboratory Report CER63-ELP-JEC9, Colorado State University, Fort Collins, Colorado.



## REFERENCES (continued)

- Sandborn, V. A. (1972) Resistance Temperature Transducers, Metrology Press, 545 pp.
- Schlichting, H. (1968) Boundary Layer Theory, McGraw Hill, New York.
- Skinner, G. T. and Ludwig, G. R. (1978) "Physical Modeling of Dispersion In the Atmospheric Boundary Layer," Calspan Advanced Technology Center, Calspan Report No. 201, May.
- Snyder, W. H. (1972) "Similarity Criteria for the Application of Fluid Models to the Study of Air Pollution Meteorology," Boundary Layer Meteorology, Vol. 3, No. 1, September.
- TSI Technical Bulletin 20 - TSI Split Film Sensor Calibration and Applications. Thermo Systems Inc., St. Paul, Minnesota.
- Van Ulden, A. P. (1974) "On the Spreading of a Heavy Gas Released Near the Ground," Loss Prevention and Safety Promotion Seminar, Delft, Netherlands, 6 pp.
- Zoric, D. and Sandborn, V. A. (1972) "Similarity of Large Reynolds Number Boundary Layers," Boundary-Layer Meteorology, Vol. 2, No. 3, March, pp. 326-333.

TABLE 1. SUMMARY OF CONCENTRATION TESTS  
(All results at equivalent field  
condition levels)

TEST-RUN	WIND TUNNEL	MODEL SCALE	WIND DIRECTION (true North) reference	STABILITY (Pasquill- Gifford)	WIND SPEED (m/s @ 2 m)	SOURCE DESCRIPTION			
						LNG Spill Volume (m <sup>3</sup> )	Spill Duration (s)	Boiloff Rate (kg/s)	Pool Dia. (m)
1-1	MET	1:170	225°	D	2.2	5.95	75	33.6	15.3
1-2	"	"	"	"	4.4	"	"	"	"
1-3	"	"	"	"	8.9	"	"	"	"
1-4	"	"	270°	"	2.2	"	"	"	"
1-5	"	"	"	"	4.4	"	"	"	"
2-1	EWT	1:85	225°	"	2.3	5.95	75	33.6	20
2-2	"	"	"	"	2.3	-	-	"	"
2-5	"	"	"	"	8.7	5.95	75	"	"
2-6	"	"	"	"	8.7	-	-	"	"
3-1	"	no model	-	"	6.7	4.39	67	27.7	"
3-2	"	"	-	"	5.1	5.2	59	37.4	"
3-3	"	1:85	203°	"	6.7	4.39	67	27.7	"
3-4	"	"	233°	"	5.1	5.2	59	37.4	"
LNG-18	"	"	214°	"	6.7	4.39	67	27.7	"
LNG-19	"	"	260°	"	5.1	5.2	59	37.4	"
LNG-20	"	"	256°	"	12.4	4.5	77	24.8	"
LNG-21	"	"	224°	"	4.9	4.2	53	33.6	"

\*MET Meteorological Wind Tunnel  
EWT Environmental Wind Tunnel

TABLE 2. PROTOTYPE CONDITIONS

CHARACTERISTICS		LNG Test No.			
		18	19	20	21
Release Diameter, D	(m)	20	20	20	20
Total Release Volume, $V_{LNG}$	( $\text{m}^3$ )	4.39	5.2	4.5	4.2
$V_{LNG}$ @ boiloff temp.	( $\text{m}^3$ )	1000	1184.5	1025	956.7
Spill Duration, $\Delta t$	(sec)	67	59	77	53
Boiloff Rates, $\dot{m}$	( $\frac{\text{kg}}{\text{sec}}$ )	27.7	37.4	24.8	33.6
$\dot{Q}$ @ boiloff temp.	( $\frac{\text{m}^3}{\text{s}}$ )	14.9	20.1	13.3	18.0
Specific Gravity @ boiloff temp.		1.55	1.55	1.55	1.55
Wind Speed, $\bar{U}$ @ 2 m	( $\frac{\text{m}}{\text{s}}$ )	6.7	5.1	12.4	4.9
Wind Direction		214°	260°	256°	224°
Stability (Pasquill-Gifford Category)		C	C-D	D	C
Humidity	(%)	16	29	15	21
Density Ratio, $\left(\frac{\rho_{LNG} - \rho_{air}}{\rho_{air}}\right)$ @ boiloff temp.	**	0.55	0.55	0.55	0.55
Reynolds No., $\left(\frac{U D}{\nu}\right)$ @ 2 m		$8.8 \times 10^6$	$6.7 \times 10^6$	$1.6 \times 10^7$	$6.4 \times 10^6$
Froude No., $\left(\frac{U^2}{g \frac{\Delta \rho}{\rho} D}\right)$ @ 2 m		0.42	0.24	1.42	0.22
Richardson No., $\frac{(T_{10m} - T_{2m}) g \Delta H}{T_{5m} (\bar{U}_{10m} - \bar{U}_{2m})^2}$		-0.15	-0.06	-	-0.11

\* For source release conditions see Figure 12.

\*\* At the 10 meter tower

\*\*\*  $T_{b.o.} = 111.63^\circ\text{K}$ ,  $\rho_{LNG} = 422.63 \frac{\text{kg}}{\text{m}^3}$ ,  $\rho_{NG}$  @ boiloff =  $1.86 \frac{\text{kg}}{\text{m}^3}$  $\nu_a = 1.526 \times 10^{-5} \text{ m}^2/\text{s}$ ,  $\rho_a = 1.197 \frac{\text{kg}}{\text{m}^3}$

TABLE 3. MODEL CONDITIONS

CHARACTERISTICS	LNG Test No.			
	18	19	20	21
Length Scale Ratio, $\frac{L_p}{L_m}$	85	85	85	85
Release Diameter, D	23.5 (cm)	23.5	23.5	23.5
Total Release Volume, $\bar{V}$	1628 (cc)	1929	1669	1558
Boiloff Duration, $\Delta t$	8.7 (sec)	7.7	10.8	6.9
Boiloff Rate, Q	186 (ccs)	251	166	225
Specific Gravity	1.38	1.38	1.38	1.38
Wind Speed, $\bar{U}$ @ 2.4 cm	60 ( $\frac{cm}{s}$ )	46	112	44
Wind Direction	214°	260°	256°	224°
Stability (Pasquill-Gifford Category)	D	D	D	D
Density Ratio, $\left(\frac{\rho_{Ar} - \rho_a}{\rho_a}\right)$	0.38	0.38	0.38	0.38
Reynolds No., $\left(\frac{\bar{U}D}{\nu}\right)$ @ 2.4 cm	9,409	7,100	17,200	6,900
Froude No., $\left(\frac{\bar{U}^2}{g \frac{\Delta \rho}{\rho} D}\right)$ @ 2.4 cm	0.42	0.24	1.43	0.23
Richardson No., $\Delta T g \Delta H / T (AU)^2$	0	0	0	0

$$\rho_{Ar} = 1.65 \frac{kg}{m^3}$$

TABLE 4. COMPARISON OF SIMILAR LNG TESTS AT DIFFERENT MODEL SCALES

x** (m)	WIND DIR.	WIND SPEED (m/s)	* x 1:170	WIND DIR.	WIND SPEED (m/s)	* x <sub>1:85</sub>
23.0	SW	2.2		SW	2.3	
28.0	"	"	14.7	"	"	32.5
45.0	"	"	12.5	"	"	21.5
63.0	"	"	5.2	"	"	
68.5	"	"		"	"	11.3
91.5	"	"		"	"	10.4
23.0	SW	8.9		SW	8.7	
28.0	"	"	23.1	"	"	24.7
45.0	"	"	11.3	"	"	20.1
63.0	"	"	8.0	"	"	
68.5	"	"		"	"	8.4
91.5	"	"		"	"	7.0
23.0	W	2.2		SW	2.3	
28.0	"	"	23.1	"	"	32.5
45.0	"	"	14.7	"	"	21.5
63.0	"	"	12.5	"	"	
63.0	"	"		"	"	11.3
91.5	"	"		"	"	10.4

\*Data taken with hot film aspirating probe

\*\*(y = 0, z = 0)

TABLE 5-1. SUMMARY OF CONCENTRATION DATA

Position			Maximum Peak Concentration (%)	Time of Arrival (sec)	Time of Peak (sec)	Approximate Time of Passage (sec)
x (m)	y (m)	z (m)				
<u>Test-Run No. 1-1</u>						
27.0	0	0	14.7	36.9	147.6	393.6
44.0	0	0	12.5	49.2	159.9	528.9
61.0	0	0	5.2	61.5	203.0	639.6
<u>Test-Run No. 1-2</u>						
27.0	0	0	26.0	24.6	116.9	184.5
44.0	0	0	14.7	18.5	86.1	258.3
61.0	0	0	13.6	24.6	129.2	393.6
<u>Test-Run No. 1-3</u>						
27.0	0	0	23.1	18.5	98.4	147.6
44.0	0	0	11.3	18.5	86.1	147.6
61.0	0	0	8.0	12.3	73.8	110.7
<u>Test-Run No. 1-4</u>						
27.0	0	0	23.1	12.3	49.2	221.4
44.0	0	0	14.7	12.3	49.2	215.3
61.0	0	0	12.5	43.1	159.9	282.9
<u>Test-Run No. 1-5</u>						
27.0	0	0	26.0	24.6	98.4	196.8
44.0	0	0	19.0	30.8	110.7	209.1
61.0	0	0	13.6	36.9	110.7	178.4

TABLE 5-2. SUMMARY OF CONCENTRATION DATA

Position			Maximum Peak Concentration (%)	Time of Arrival (sec)	Time of Peak (sec)	Approximate Time of Passage (sec)
x <sup>*</sup> (m)	y (m)	z (m)				
<u>Test-Run No. 2-1</u> (Wind Direction = 225°)*						
29.9	0	0	32.5	26.7	91.5	213.5
54.9	-17.1	0	11.8	61.0	160.2	266.9
45.8	0	0	21.5	30.5	110.6	278.4
68.9	0	0	11.3	22.9	129.6	373.7
91.5	0	0	10.4	95.1	152.5	274.5
42.1	-17.7	0	19.4	30.5	99.1	266.9
63.4	-26.2	0	12.0	76.3	125.9	240.3
42.1	17.7	0	26.0	45.8	133.5	213.5
<u>Test-Run No. 2-2</u> (Wind Direction = 225°)*						
29.9	0	0	43.5			
54.9	-17.1	0	22.3			
45.8	0	0	28.2			
68.9	0	0	19.2			
91.5	0	0	14.7			
42.1	-17.7	0	28.4			
63.4	-26.2	0	16.7			
<u>Test-Run No. 2-5</u> (Wind Direction = 225°)*						
29.9	0	0	24.7	7.6	80.1	137.3
54.9	-17.1	0	0.5	72.5	80.1	106.8
45.8	0	0	20.1	11.5	61.0	137.3
68.9	0	0	8.4	26.7	64.9	114.4
91.5	0	0	7.0	45.8	68.6	129.6
42.1	-17.7	0	0.3	72.5	76.3	80.1
42.1	17.7	0	21.3	22.9	53.4	129.6
63.4	26.2	0	14.3	0	0	0
<u>Test-Run No. 2-6</u> (Wind Direction = 225°)*						
29.9	0	0	27.1			
54.9	-17.1	0	1.1			
45.8	0	0	21.3			
68.9	0	0	12.0			
91.5	0	0	6.7			
42.1	-17.7	0	1.6			
63.4	-26.2	0	0.5			
42.1	17.7	0	24.1			

\*Coordinate system is right handed and the positive x-axis is orientated in the direction of the wind. Wind direction is reference to direction wind comes from.

TABLE 5-3. SUMMARY OF CONCENTRATION DATA

Test-Run No. 3-1

Position			Maximum Peak Concentration (%)	Time of Arrival (sec)	Time of Peak (sec)	Approximate Time of Passage (sec)
x (m)	y (m)	z (m)				
18.5	0	0	33.9	9.6	65.0	162.6
18.5	8.5	0	49.0	9.6	68.9	99.5
18.5	-8.5	0	33.9	13.4	68.9	95.6
27.0	0	0	29.0	9.6	51.6	65.0
27.0	-8.5	0	31.2	11.5	44.0	114.8
35.5	0	0	27.1	13.4	51.6	166.4
35.5	8.5	0	27.2	13.4	76.5	114.8
35.5	-8.5	0	32.5	15.3	74.6	139.6
44.0	0	0	25.5	17.2	66.9	153.0
52.5	0	0	22.6	17.2	65.0	172.1
52.5	8.5	0	17.0	13.4	68.9	118.6
52.5	-8.5	0	17.1	17.2	66.9	122.4
61.0	0	0	20.5	15.3	61.2	147.3
61.0	17.0	0	12.0	28.1	49.1	137.7
61.0	-17.0	0	0.46	47.8	47.8	47.8
69.5	0	0	15.3	19.1	63.1	172.1
69.5	8.5	0	15.1	17.2	65.0	137.7
69.5	-8.5	0	17.8	19.1	76.5	143.5
78.0	0	0	15.1	19.1	72.7	174.1
86.5	0	0	12.4	19.1	76.5	153.0
86.5	8.5	0	11.7	19.1	84.2	120.5
86.5	-8.5	0	15.7	21.0	72.7	153.0
95.0	0	0	11.0	19.1	65.0	133.9
103.5	0	0	12.5	26.8	63.1	172.1
103.5	8.5	0	9.8	24.9	66.9	124.3
103.5	-8.5	0	8.6	26.8	57.4	114.8
112.0	0	0	8.2	28.7	93.7	122.4
112.0	17.0	0	8.0	30.6	88.0	133.9
111.8	25.5	0	1.6	49.7	53.6	65.0
112.0	-17.0	0	2.1	40.2	44.0	57.4
120.5	0	0	10.9	23.0	88.0	154.9
120.5	8.5	0	9.0	28.7	86.1	158.8
120.5	-8.5	0	9.5	42.1	80.3	139.6
129.0	0	0	8.9	30.6	91.8	166.4
137.5	0	0	9.3	36.3	70.8	135.8
137.5	8.5	0	6.9	51.6	78.4	114.8
137.5	-8.5	0	7.7	30.6	72.7	133.9
146.0	0	0	5.9	34.4	59.3	133.9



TABLE 5-3. (continued)

Test-Run No. 3-2

Position			Maximum Peak Concentration (%)	Time of Arrival (sec)	Time of Peak (sec)	Approximate Time of Passage (sec)
x (m)	y (m)	z (m)				
18.5	0	0	48.7	9.6	67.0	136.0
27.0	0	0	42.8	15.3	70.9	105.3
27.0	12.8	0	38.5	11.5	51.7	111.1
27.0	25.5	0	0.0	0	0	0
27.0	-12.8	0	9.9	53.6	57.5	61.3
27.0	-25.5	0	0.0	0	0	0
44.0	0	0	34.5	21.1	53.6	149.4
61.0	0	0	24.4	19.2	72.8	134.1
61.0	12.8	0	25.2	19.2	74.7	141.7
61.0	25.5	0	1.55	26.8	28.7	30.6
61.0	-12.8	0	18.6	63.2	76.6	86.2
61.0	-25.5	0	0	0	0	0
78.0	0	0	22.1	23.0	68.9	141.7
95.0	0	0	18.3	38.3	76.6	137.9
112.0	0	0	14.5	32.6	80.4	143.6
112.0	12.8	0	13.7	28.7	95.8	162.8
112.0	25.5	0	6.8	44.0	80.4	107.2
112.0	-12.8	0	6.1	51.7	84.3	120.6
112.0	-25.5	0	0.0	0	0	0
129.0	0	0	12.4	38.3	86.2	153.2

TABLE 5-3. (continued)

Test-Run No. 3-3 (Wind Direction = 203°)\*

Position			Maximum Peak Concentration (%)	Time of Arrival (sec)	Time of Peak (sec)	Approximate Time of Passage (sec)
x (m)	y (m)	z (m)				
22.5	0	0	30.9	11.5	38.3	141.5
22.5	8.5	0	22.5	15.3	42.1	97.6
22.5	17.0	0	5.8	45.9	89.9	93.7
22.5	-8.5	0	19.6	15.3	44.0	124.3
22.5	-17.0	0	4.9	32.5	36.3	42.1
22.5	-25.5	0	0.2	0	0	0
35.3	0	0	13.2	23.0	65.0	118.6
35.3	12.8	0	14.8	34.4	45.9	120.5
43.8	0	0	13.8	17.2	68.9	137.7
43.8	-17.0	0	6.7	30.6	80.3	114.8
48.0	0	0	12.9	19.1	59.3	130.1
48.0	8.5	0	15.8	23.0	86.1	133.9
48.0	17.0	0	4.6	19.1	59.3	89.9
48.0	25.5	0	1.6	66.9	68.9	78.4
48.0	-8.5	0	9.0	23.0	68.9	120.5
48.0	-17.0	0	4.6	23.0	61.2	93.7
48.0	-25.5	0	1.0	42.1	44.0	49.7
56.5	4.3	0	8.18	19.1	47.8	97.6
60.8	0	0	6.7	26.8	57.4	110.9
73.5	0	0	7.3	24.9	49.7	114.8
73.5	8.5	0	7.3	23.0	57.4	137.7
73.5	17.0	0	4.0	24.9	36.3	78.4
73.5	25.5	0	1.6	45.9	66.9	89.9
73.5	34.0	0	0.1	0	0	0
73.5	-8.5	0	5.8	24.9	80.3	114.8
73.5	-17.0	0	3.4	24.9	51.6	86.1
73.5	-25.5	0	3.7	61.2	72.7	118.6
73.5	-34.0	0	0.1	0	0	0
86.3	0	0	6.1	24.9	93.7	137.7
86.3	8.5	0	5.8	23.0	49.7	133.9
86.3	17.0	0	4.3	23.0	99.5	122.4
86.3	25.5	0	2.7	51.6	59.3	105.2
86.3	34.0	0	1.1	66.9	80.3	88.0
86.3	-8.5	0	6.1	23.0	61.2	126.2
86.3	-17.0	0	1.9	45.9	80.3	114.8
107.5	0	0	7.0	23.0	70.8	154.9
107.5	8.5	0	5.1	23.0	74.6	137.7
107.5	17.0	0	6.1	44.0	72.7	141.5
107.5	25.5	0	1.9	45.9	95.6	105.2
107.5	34.0	0	1.1	36.3	51.6	57.4
107.5	-8.5	0	4.2	49.7	84.2	149.2
107.5	-17.0	0	2.2	51.6	107.1	137.7

\*Coordinate system is right handed and the positive x-axis is orientated in the direction of the wind. Wind direction is reference to direction wind comes from.

TABLE 5-3. (continued)

Test-Run No. 3-3 (continued) Wind Direction = 203°)\*

Position			Maximum Peak Concentration (%)	Time of Arrival (sec)	Time of Peak (sec)	Approximate Time of Passage (sec)
x (m)	y (m)	z (m)				
107.5	-25.5	0	1.1	49.7	72.7	80.3
120.3	0	0	7.4	30.6	74.6	141.5
120.3	8.5	0	6.4	36.3	68.9	145.4
120.3	17.0	0	4.5	30.6	82.2	130.1
120.3	25.5	0	3.0	28.7	101.4	120.5
120.3	34.0	0	1.7	68.9	86.1	103.3
120.3	42.5	0	0.5	76.5	76.5	76.5
120.3	-8.5	0	5.4	28.7	74.6	147.3
120.3	-17.0	0	1.7	34.4	76.5	126.2
120.3	-25.5	0	0.3	0	0	0
145.8	0	0	3.2	28.7	66.9	137.7
145.8	17.0	0	2.5	34.4	86.1	133.9
145.8	34.0	0	0.0	0	0	0

\*Coordinate system is right handed and the positive x-axis is orientated in the direction of the wind. Wind direction is reference to direction wind comes from.

TABLE 5-3. (continued)

Test-Run No. 3-4 (Wind Direction = 233°)\*

Position			Maximum Peak Concentration (%)	Time of Arrival (sec)	Time of Peak (sec)	Approximate Time of Passage (sec)
x (m)	y (m)	z (m)				
22.5	0	0	28.2	17.2	53.6	113.0
22.5	8.5	0	18.5	13.8	76.6	113.0
22.5	17.0	0	2.0	23.0	24.9	28.7
22.5	-8.5	0	37.6	11.5	57.5	111.1
22.5	-17.0	0	7.4	24.9	67.0	74.7
22.5	-25.5	0	0.2	0	0	0
35.3	0	0	27.2	23.0	76.6	115.0
35.3	0	0	28.4	15.3	65.1	145.5
48.0	0	0	17.5	15.3	452.0	153.2
60.8	0	0	17.0	19.6	78.5	143.6
60.8	8.5	0	12.6	38.3	67.0	113.0
60.8	17.0	0	8.2	46.0	88.1	124.5
60.8	25.5	0	0.0	0	0	0
60.8	-8.5	0	15.3	21.1	70.9	137.9
60.8	-17.0	0	12.9	19.6	55.5	105.3
60.8	-25.5	0	6.8	26.8	30.6	63.2
60.8	-34.0	0	0.5	46.0	47.9	47.9
73.5	0	0	14.6	21.1	76.6	118.7
86.3	0	0	13.0	24.9	72.8	134.1
86.3	8.5	0	12.5	28.7	76.6	172.4
86.3	17.0	0	8.7	38.3	84.3	114.9
86.3	25.5	0	5.4	42.1	88.1	143.6
86.3	34.0	0	0.3	0	0	0
86.3	-8.5	0	10.3	30.6	57.5	134.1
86.3	-17.0	0	5.2	42.1	63.2	120.6
86.3	-25.5	0	1.4	80.4	84.3	103.4
86.3	-34.0	0	0.2	0	0	0
99.0	0	0	9.0	24.9	82.3	149.4
99.0	8.5	0	5.1	34.5	91.9	157.0
99.0	17.0	0	7.8	46.0	61.3	137.9
99.0	25.5	0	4.6	49.8	65.1	141.7
99.0	34.0	0	1.1	61.3	74.7	80.4
99.0	-8.5	0	9.4	26.8	72.8	156.0
99.0	-17.0	0	8.1	47.9	61.3	134.1
99.0	-25.5	0	3.9	80.4	88.1	120.6
99.0	-34.0	0	0.3	0	0	0
111.8	0	0	7.6	32.6	72.8	151.3
124.5	0	0	7.9	26.8	76.6	153.2
124.5	8.5	0	7.4	38.3	80.4	172.4
124.5	17.0	0	1.1	91.9	99.6	126.4
124.5	25.5	0	0.8	49.8	99.6	126.4
124.5	-8.5	0	8.7	46.0	84.3	153.2
124.5	-17.0	0	5.8	34.5	76.6	134.1
124.5	-25.5	0	0.3	0	0	0

\*Coordinate system is right handed and the positive x-axis is orientated in the direction of the wind. Wind direction is reference to direction wind comes from.

TABLE 5-3. (continued)

Test-Run No. 3-4 (continued) (Wind Direction = 233°)\*

Position			Maximum Peak Concentration (%)	Time of Arrival (sec)	Time of Peak (sec)	Approximate Time of Passage (sec)
x (m)	y (m)	z (m)				
137.3	0	0	6.8	34.5	76.6	145.5
137.3	8.5	0	7.8	38.3	76.6	180.0
137.3	17.0	0	3.6	49.8	84.3	145.5
137.3	25.5	0	0.0	0	0	0
137.3	-8.5	0	6.7	34.5	88.1	153.2
137.3	-17.0	0	5.2	72.8	84.3	149.4
137.3	-25.5	0	4.5	42.1	91.9	134.1
137.3	-34.0	0	0.0	0	0	0

\*Coordinate system is right handed and the positive x-axis is orientated in the direction of the wind. Wind direction is reference to direction wind comes from.

TABLE 5-4. SUMMARY OF CONCENTRATION DATA

Test-Run No. LNG-18 (Wind Directions - 214°)\*

China Lake Naval Wea- pons Grid Test Posi- tion No.	Position			Maximum Peak Concentration (%)	Time of Arrival (sec)	Time of Peak (sec)	Approximate Time of Passage (sec)
	x (m)	y (m)	z (m)				
	22.5	0	0	48.0	5.7	38.3	68.9
	32.7	0	0	30.4	9.6	38.3	53.6
	45.5	0	0	20.6	7.7	26.8	65.1
	58.2	0	0	17.3	7.7	34.5	57.5
	71.0	0	0	11.6	11.5	36.4	76.6
	83.7	0	0	9.5	11.5	34.4	70.9
	96.5	0	0	8.6	11.5	42.1	82.3
	96.5	44.2	1.5	0.0	0	0	0
	105.0	-5.1	1.5	5.5	15.3	19.2	47.9
	109.2	0	0	5.9	11.5	30.6	70.9
	122.0	0	0	6.9	15.3	47.9	76.6
	134.7	0	0	4.7	13.4	42.1	76.6
1	47.9	11.1	1.5	0.0	9.6	30.6	53.6
2	47.9	11.1	1.5	5.9	11.5	21.1	53.6
3	75.3	17.0	1.5	0.0	11.5	32.5	68.9
4	75.3	17.0	1.5	4.0	11.5	38.3	55.5
5	99.9	20.4	0.5	3.6	19.2	46.0	65.1
6	124.5	25.5	1.5	1.7	17.2	30.6	76.6
7	54.0	-15.3	1.5	7.6	13.4	34.5	49.8
8	80.3	-53.6	1.5	6.4	15.3	38.3	76.6
9	45.5	34.9	1.5	0.0	0	0	0
10	71.0	39.1	1.5	0.0	0	0	0

Test-Run No. LNG-19 (Wind Direction = 260°)\*

China Lake Naval Wea- pons Grid Test Posi- tion No.	Position			Maximum Peak Concentration (%)	Time of Arrival (sec)	Time of Peak (sec)	Approximate Time of Passage (sec)
	x (m)	y (m)	z (m)				
	22.5	0	0	48.0	3.8	34.5	49.8
	32.7	0	0	34.6	7.7	23.0	65.1
	45.5	0	0	27.2	7.7	26.8	57.5
	58.2	0	0	24.3	11.5	34.5	65.1
	71.0	0	0	15.8	11.5	42.1	88.1
	83.7	0	0	15.2	15.3	26.8	72.8
	96.5	0	0	13.2	19.2	42.1	84.3
	98.2	-36.6	1.5	0.0	0	0	0
	109.2	0	0	11.4	11.5	38.3	72.8
	122.0	0	0	11.4	15.3	38.3	72.8
	134.7	0	0	7.8	15.3	38.3	76.6
2	42.1	-28.9	0.5	0.0	0	0	0
9	55.7	-8.5	1.5	20.3	7.7	34.5	65.1
10	77.8	-23.0	1.5	0.0	0	0	0

\*Coordinate System is right handed and the positive x-axis is orientated in the direction of the wind. Wind Direction is reference to direction wind comes from.

TABLE 5-4. (continued)

Test-Run No. LNG-20 (Wind Direction = 256°)\*

China Lake Naval Weapons Grid Test Position No.	Position			Maximum Peak Concentration (%)	Time of Arrival (sec)	Time of Peak (sec)	Approximate Time of Passage (sec)
	x (m)	y (m)	z (m)				
	22.5	0	0	18.8	3.8	11.5	70.9
	22.5	8.5	0	3.9	7.7	19.2	68.9
	22.5	17.0	0	0.0	0	0	0
	22.5	-8.5	0	9.7	5.8	24.9	68.9
	22.5	-17.0	0	0.0	0	0	0
	32.7	0	0	15.2	3.8	23.0	72.8
	32.7	8.5	0	4.4	7.7	34.5	84.3
	32.7	-8.5	0	8.6	5.8	42.1	80.4
	32.7	-17.0	0	0.0	0	0	0
	45.5	0	0	9.5	5.8	26.8	84.3
	45.5	8.5	0	5.6	5.8	11.5	67.0
	45.5	-8.5	0	5.6	7.7	34.5	72.8
	45.5	-17.0	0	0.0	0	0	0
	58.2	0	0	7.8	7.7	36.4	76.6
	58.2	8.5	0	5.9	5.8	26.8	72.8
	58.2	17.0	0	1.1	13.4	23.0	51.7
	58.2	-8.5	0	5.1	11.5	42.1	68.9
	58.2	-17.0	0	0.5	28.7	28.7	28.7
	71.0	0	0	6.4	7.7	38.3	72.8
	71.0	8.5	0	5.4	7.7	38.3	76.6
	71.0	17.0	0	1.6	13.4	40.2	57.5
	71.0	25.5	0	0.5	34.5	38.3	49.8
	71.0	-8.5	0	3.6	15.3	30.6	32.6
	71.0	-17.0	0	0.0	0	0	0
	83.7	0	0	4.4	7.7	38.3	76.6
	83.7	8.5	0	3.9	5.8	26.8	111.1
	83.7	17.0	0	1.8	11.5	23.0	65.1
	83.7	25.5	0	0.5	23.0	26.8	30.6
	83.7	-8.5	0	2.9	11.5	21.1	74.7
	83.7	-17.0	0	0.5	23.0	24.9	26.8
	96.5	0	0	4.4	7.7	42.1	91.9
	96.5	8.5	0	3.6	7.7	46.0	91.9
	96.5	17.0	0	1.6	11.5	46.0	65.1
	96.5	25.5	0	0.3	95.8	103.4	122.6
	96.5	-8.5	0	3.1	11.5	38.3	80.4
	96.5	-17.0	0	0.0	0	0	0
	100.7	-28.9	1.5	0.0	0	0	0
	109.2	0	0	3.4	7.7	42.1	91.9
	109.2	8.5	0	3.3	7.7	38.3	88.1
	109.2	17.0	0	1.6	11.5	46.0	68.9
	109.2	25.5	0	0.8	26.8	30.6	34.5
	109.2	-8.5	0	2.6	7.7	30.6	68.9
	109.2	-17.0	0	0.3	38.3	42.1	42.1
	122.0	0	0	2.9	7.7	38.3	80.4
	134.7	0	0	2.1	7.7	46.0	95.8
2	43.8	-25.5	0.5	0.0	0	0	0
4	64.2	-39.1	1.5	0.0	0	0	0
9	56.5	-4.3	1.5	8.8	5.8	40.2	99.6
10	86.3	-15.3	1.5	2.5	3.8	23.0	26.8

\*Coordinate System is right handed and the positive x-axis is orientated in the direction of the wind. Wind Direction is reference to direction wind comes from.

TABLE 5-4. (continued)

Test-Run No. LNG-21 (Wind Direction = 224°)\*

China Lake Naval Weapons Grid Test Position No.	Position			Maximum Peak Concentration (%)	Time of Arrival (sec)	Time of Peak (sec)	Approximate Time of Passage (sec)
	x (m)	y (m)	z (m)				
	22.5	0	0	51.9	3.83	30.6	76.6
	22.5	8.5	0	46.4	3.83	11.5	49.8
	22.5	17.0	0	5.6	0	0	0
	22.5	25.5	0	0.0	0	0	0
	22.5	-8.5	0	41.3	7.7	32.6	65.1
	22.5	-17.0	0	21.2	28.7	30.6	34.5
	22.5	-25.5	0	0.0	0	0	0
	32.7	0	0	33.6	7.7	30.6	84.3
	32.7	8.5	0	27.2	9.6	34.5	61.3
	32.7	17.0	0	17.7	15.3	28.7	72.8
	32.7	25.5	0	1.8	26.8	40.2	59.4
	32.7	-8.5	0	25.0	11.5	36.4	57.5
	32.7	-17.0	0	15.2	13.4	38.3	76.6
	32.7	-25.5	0	0.3	30.6	30.6	30.6
	45.5	0	0	28.2	9.6	42.1	72.8
	45.5	8.5	0	24.9	19.2	34.5	61.3
	45.5	17.0	0	3.6	15.3	21.1	24.9
	45.5	25.5	0	0.5	32.6	36.4	44.1
	45.5	-8.5	0	28.2	7.7	38.3	91.1
	45.5	-17.0	0	16.9	15.3	32.6	74.7
	45.5	-25.5	0	2.9	0	0	0
	58.2	0	0	20.0	13.4	34.5	74.7
	58.2	8.5	0	15.4	15.3	38.3	61.3
	58.2	17.0	0	3.1	19.2	32.6	49.8
	58.2	25.5	0	1.3	107.2	115.0	114.9
	58.2	34.0	0	0.0	0	0	0
	58.2	-8.5	0	22.4	11.5	36.4	72.8
	58.2	-17.0	0	17.5	23.0	36.4	61.3
	58.2	-25.5	0	3.9	149.4	153.2	178.1
	58.2	-34.0	0	0.0	0	0	0
	71.0	0	0	10.7	11.5	42.1	59.4
	71.0	8.5	0	16.7	19.2	28.7	51.7
	71.0	17.0	0	5.6	38.3	42.1	57.5
	71.0	25.5	0	1.1	32.6	42.1	49.8
	71.0	-8.5	0	14.9	13.4	46.0	91.9
	71.0	-17.0	0	15.6	11.5	12.6	67.0
	71.0	-25.5	0	16.2	126.4	137.9	160.9
	71.0	-34.0	0	2.6	34.5	38.3	47.9
	71.0	-42.5	0	0.0	0	0	0
	83.7	0	0	11.6	130.2	153.2	187.7
	83.7	8.5	0	13.8	21.1	47.9	80.4
	83.7	17.0	0	10.9	28.7	46.0	68.9
	83.7	25.5	0	9.0	91.9	111.1	143.6
	83.7	34.0	0	0.0	0	0	0
	83.7	-8.5	0	13.8	13.4	34.5	86.2
	83.7	-17.0	0	17.7	30.6	34.5	67.0
	83.7	-25.5	0	6.6	26.8	38.3	61.3
	83.7	-34.0	0	1.8	11.5	23.0	53.6
	96.5	0	0	12.3	11.5	40.2	99.6
	96.5	8.5	0	14.3	9.6	36.4	111.1
	96.5	17.0	0	4.4	24.9	34.5	42.1
	96.5	25.5	0	3.4	160.9	164.7	183.8
	96.5	-8.5	0	9.7	15.3	42.1	103.4
	96.5	-17.0	0	10.0	13.4	34.5	90.0
	96.5	-25.5	0	1.8	24.9	26.8	38.3
	96.5	-34.0	0	0.0	0	0	0
	101.6	27.2	1.5	1.8	0	0	0
	102.4	-23.8	1.5	8.2	17.2	46.0	68.9
	109.2	0	0	9.7	17.2	42.1	91.9
	109.2	8.5	0	9.7	19.2	51.7	82.4
	109.2	17.0	0	3.1	36.4	49.8	70.9
	109.2	25.5	0	2.6	44.1	49.8	57.5
	109.2	-8.5	0	12.3	17.2	46.0	93.8
	109.2	-17.0	0	10.6	17.2	44.1	86.2
	109.2	-25.5	0	0.0	0	0	0

\*Coordinate System is right handed and the positive x-axis is orientated in the direction of the wind. Wind Direction is reference to direction wind comes from.



TABLE 5-4. (continued)

Test-Run No. LNG-21 (Wind Direction = 224°)\*

China Lake Naval Weapons Grid Test Position No.	Position			Maximum Peak Concentration (%)	Time of Arrival (sec)	Time of Peak (sec)	Approximate Time of Passage (sec)
	x (m)	y (m)	z (m)				
	122.0	0	0	6.4	15.3	30.6	72.8
	122.0	8.5	0	5.4	23.0	34.5	72.8
	122.0	17.5	0	6.1	34.5	42.1	57.5
	122.0	25.5	0	0.8	143.6	153.2	176.2
	122.0	-8.5	0	8.3	19.2	47.9	99.6
	122.0	-17.0	0	8.8	32.6	55.5	95.8
	122.0	-25.0	0	8.2	21.1	42.1	90.0
	122.0	-34.0	0	2.1	139.8	153.2	164.7
	134.7	0	0	8.2	23.0	46.0	88.1
	134.7	8.5	0	3.6	30.6	51.7	86.2
	134.7	17.0	0	2.7	38.3	49.8	76.6
	134.7	25.5	0	0.5	51.7	53.6	68.9
	134.7	-8.5	0	8.6	19.2	57.5	134.1
	134.7	-17.0	0	8.8	19.2	51.7	124.5
	134.7	-25.5	0	6.4	46.0	42.1	88.1
	134.7	-34.0	0	2.1	38.3	48.0	76.6
1	50.6	1.7	1.5	19.0	9.6	32.6	72.8
2	50.6	1.7	0.5	24.7	11.5	40.2	118.7
3	77.8	1.7	1.5	10.5	17.2	30.6	88.1
4	77.8	1.7	0.5	17.7	13.4	30.6	99.6
5	102.4	2.6	0.5	12.3	19.2	38.3	91.9
6	127.1	2.6	1.5	6.1	15.3	34.5	86.2
7	51.4	-23.8	1.5	4.3	24.9	28.7	36.4
8	77.8	-23.8	1.5	10.8	19.2	28.7	68.9
9	50.6	27.2	1.5	4.0	9.6	42.1	67.0
10	76.9	27.2	1.5	1.5	0	0	0

\*Coordinate System is right handed and the positive x-axis is orientated in the direction of the wind. Wind Direction is reference to direction wind comes from.

TABLE 6. SUMMARY OF APPROACH FLOW CHARACTERISTICS

DESCRIPTION	ATMOSPHERIC DATA*	MODELED VALUES**
$z_o$ (m)	0.01 - 0.15	0.017
$1/n$	0.143 - 0.167	0.18
$\Lambda_x$ (m) @ 2 meters	12.0 - 30.0	14.5
$\Lambda_z$ (m) @ 2 meters	1 - 2	5.1

---

\*Counihan, 1975

\*\*At wind speed reference location (see Figure 6)

TABLE 7. SUMMARY OF PEAK CONCENTRATION DATA AT TEST POINT LOCATIONS FOR MODEL AND FIELD

Location (China Lake Naval Weapons Grid)	LNG-18		LNG-19		LNG-20		LNG-21	
	Field	Model	Field	Model	Field	Model	Field	Model
1	>5%	5.9	>5%	0	1.6%	0	1.6%	19
2	>5%	5.3	>5%	0.0	1.0	0.0	1.6%	24.7
3	>5%	4.1	0.75	0	0	0.0	0.7	10.6
4	>5%	4.0	>5%	0	0	0.0	1.6%	17.7
5	0.7	3.6	0	0	0	0.0	0.6	12.3
6	0	1.7	0	0	0	0.0	0.3	6.1
7	4.0	7.6	0	0	0	0.0	2.1	4.3
8	0	6.4	0	0	0	0	0	10.8
9	0	0	>5%	20.8	2.4%	8.8	0	4.0
10	0.3	0	>5%	0.0	1.8%	2.5	0	1.5

Location Lawrence Livermore Lab Grid)	LNG-18		LNG-19		LNG-20		LNG-21	
	Field	Model*	Field	Model*	Field	Model*	Field	Model*
1	42.5	>40.0	46.0	>50.0	22.0	>20.0	64.0	>50.0
2	41.0	>40.0	33.0	>50.0	35.0	>19.0	36.0	>50.0
3	23.0	>32.0	26.0	>10.0	-	>0.0	33.0	>35.0
4	38.0	> 7.0	21.0	>15.0	11.0	>2.5	34.0	>25.0
5	-	-	-	>0.0	-	>0.0	28.0	>27.0
6	-	-	16.4	>8	12.75	>0.8	10.5	>10.0
7	-	-	0.0	>0.0	0.6	>0.0	5.3	>12.0
8	-	-	8.1	>0.0	1.9	>0.0	-	>5.0

\*Approximate values only, model data was not obtained on the Lawrence Livermore grid sites.

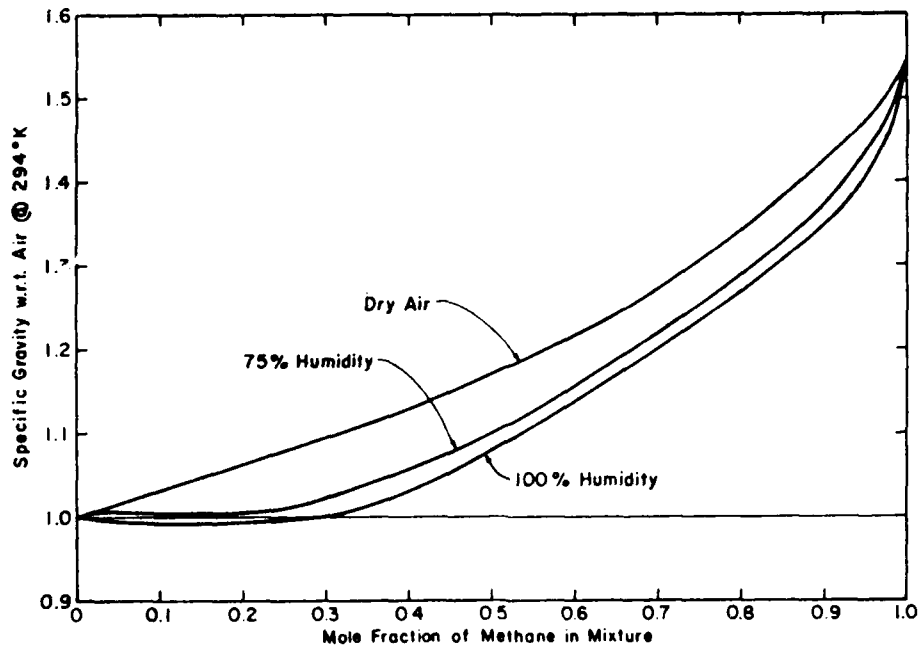


Figure 1. Specific Gravity of LNG Vapor - Humid Atmosphere Mixtures

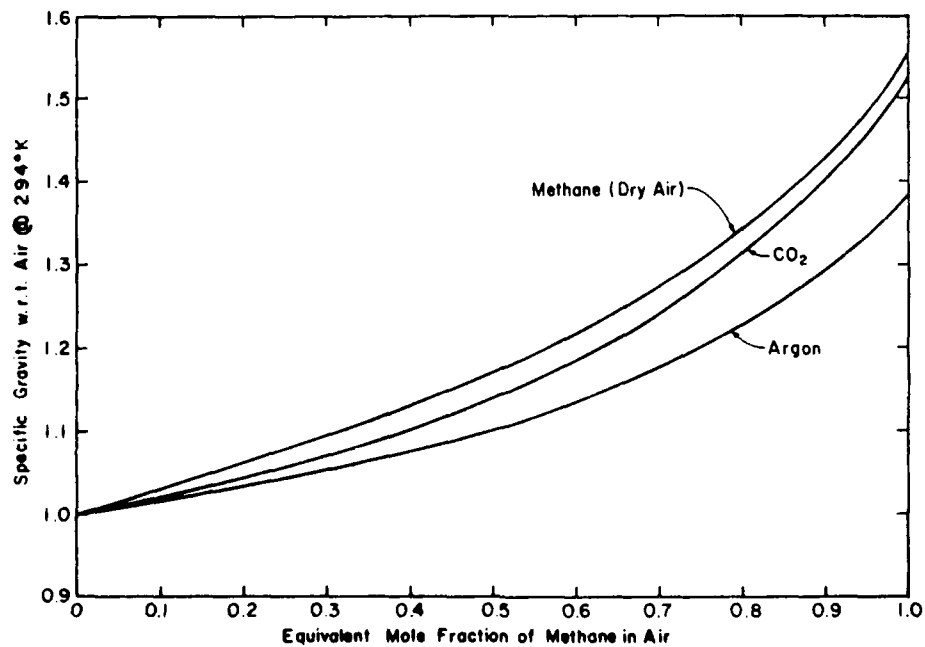


Figure 2. Specific Gravity of Gas-Air Mixtures

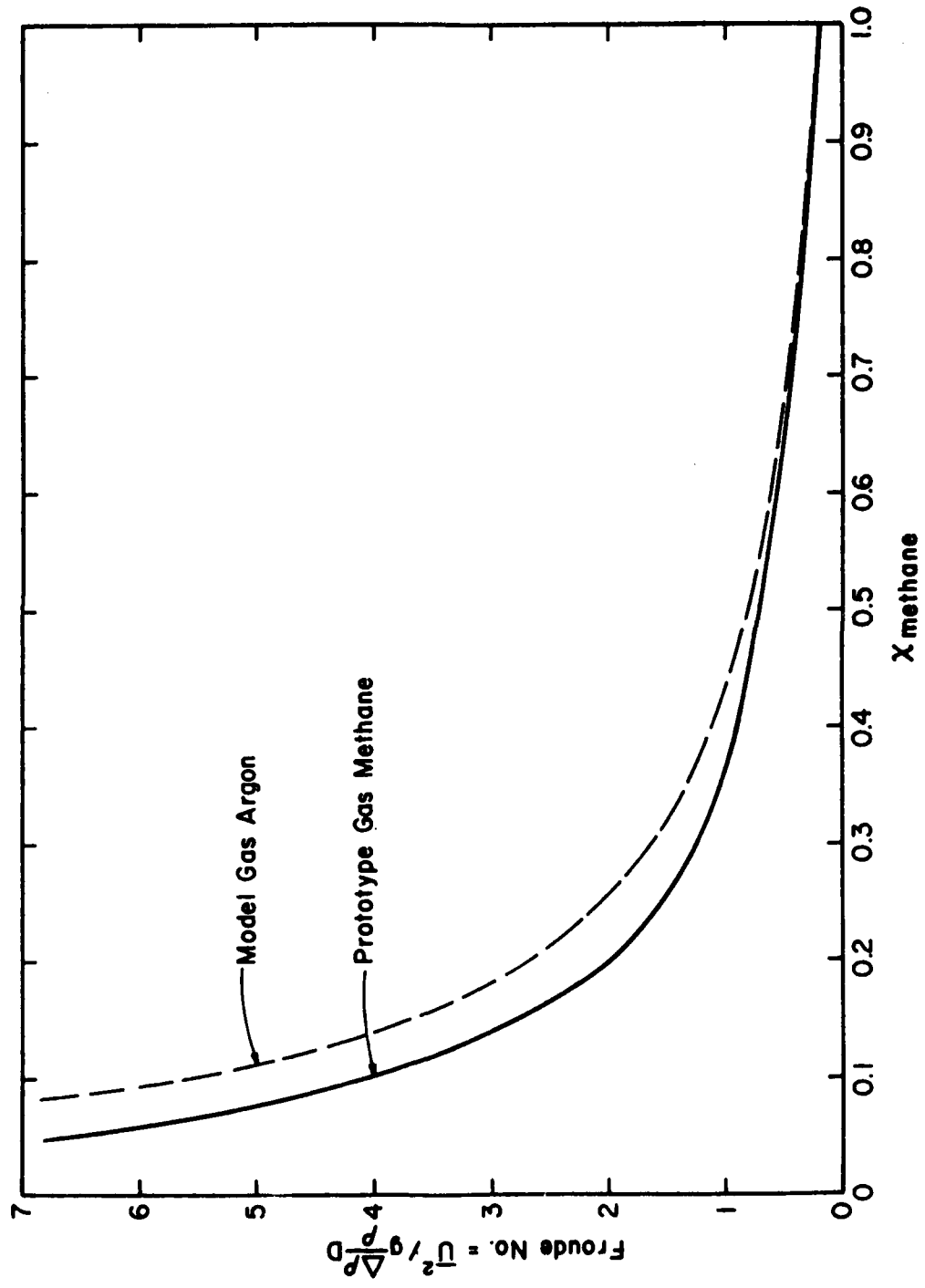


Figure 3. Variation of Froude Number for Gas-Air Mixtures

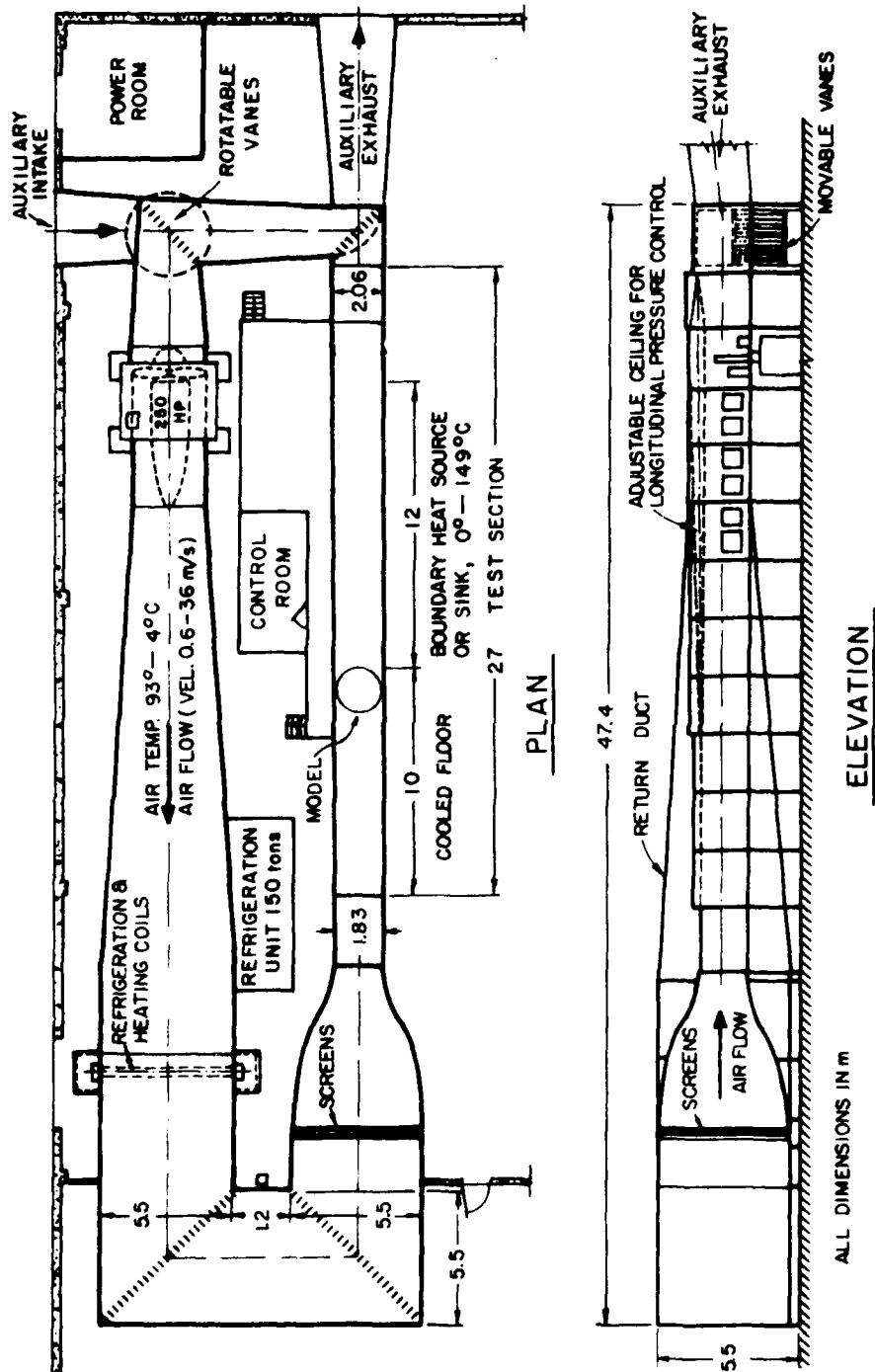


Figure 4. Meteorological Wind Tunnel

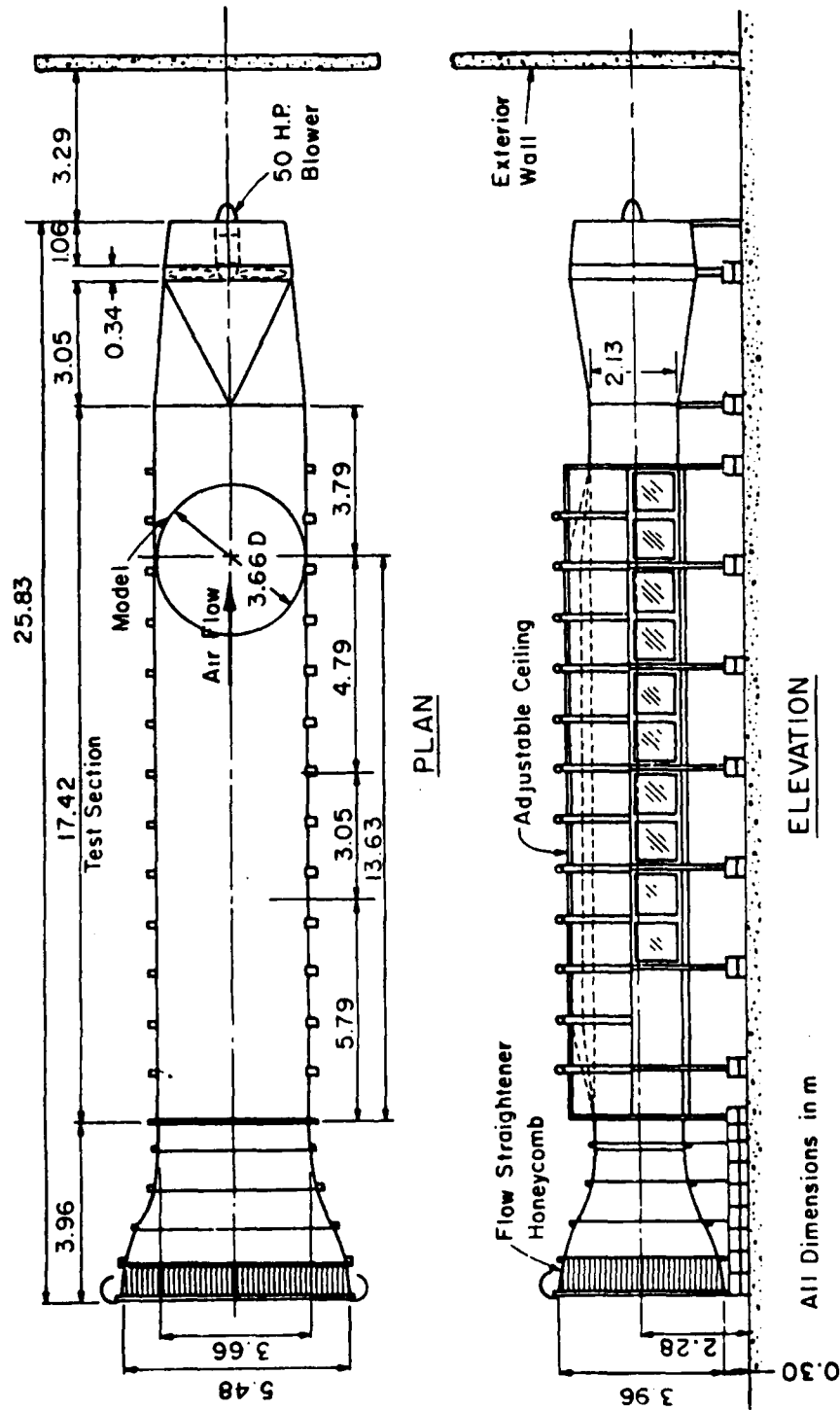


Figure 5. Environmental Wind Tunnel

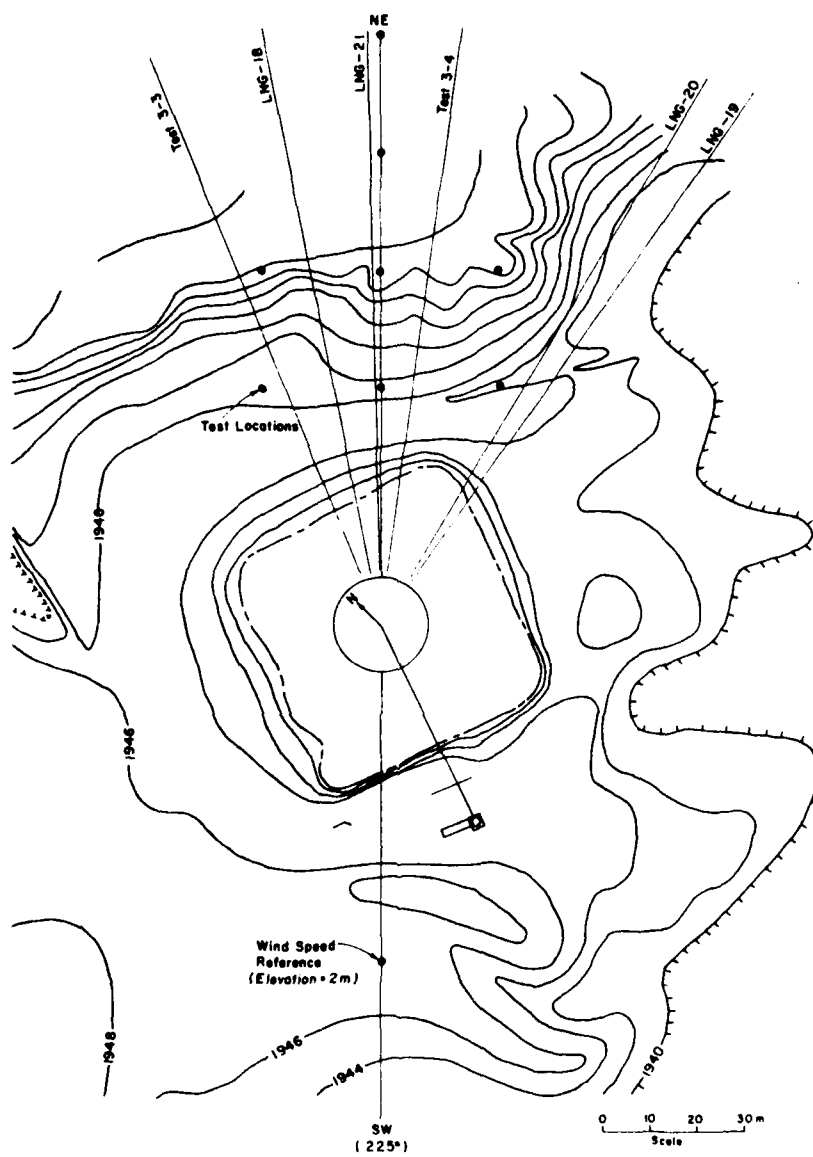


Figure 6. China Lake Test Site



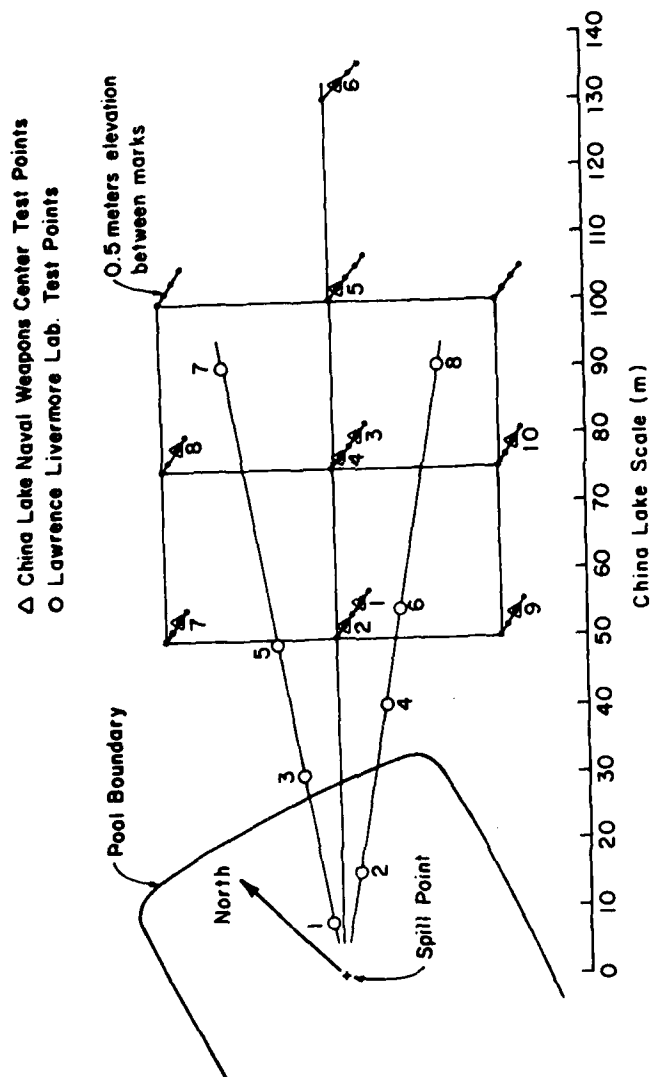


Figure 7. Field Concentration Measurement Locations

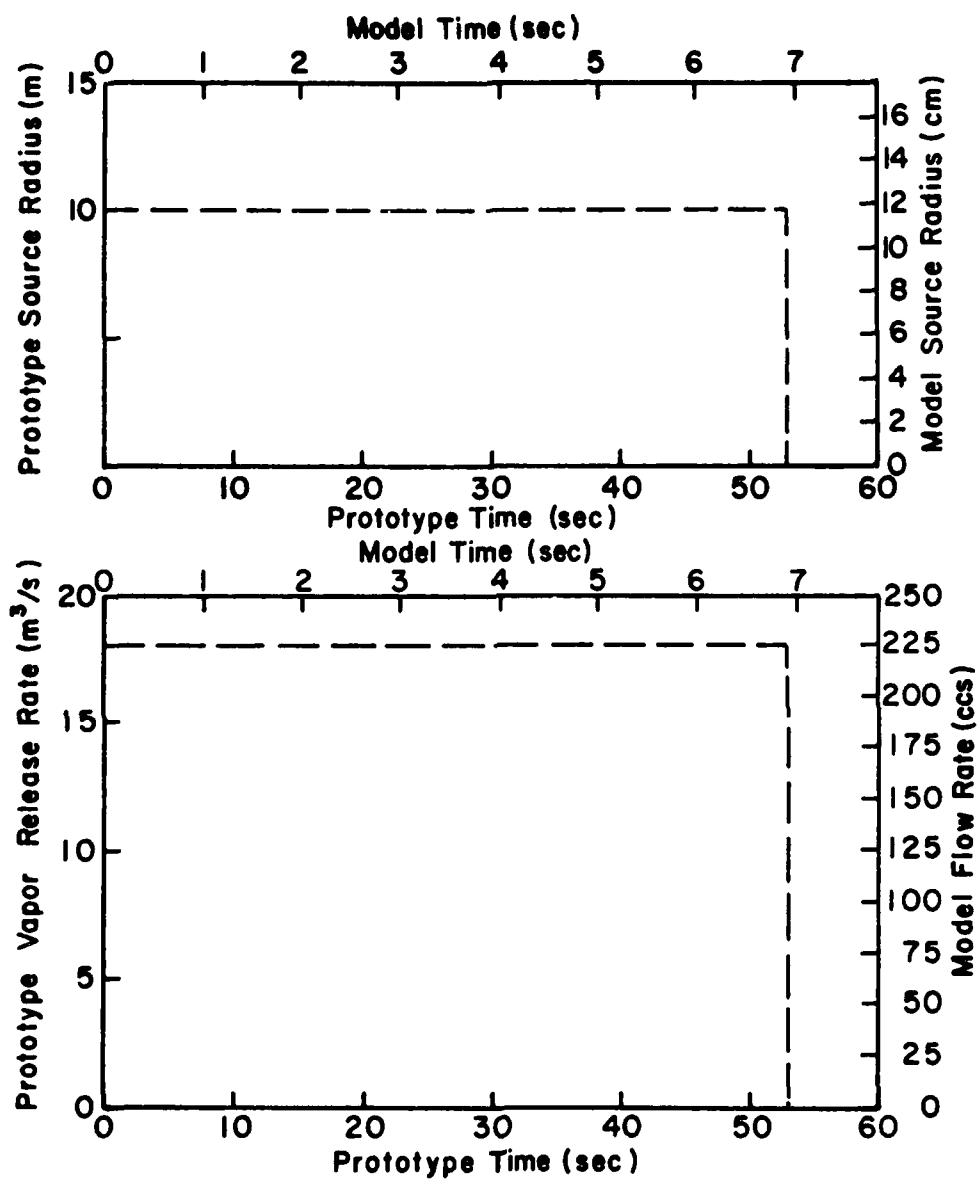


Figure 8. Model and Prototype Source Conditions for LNG-21

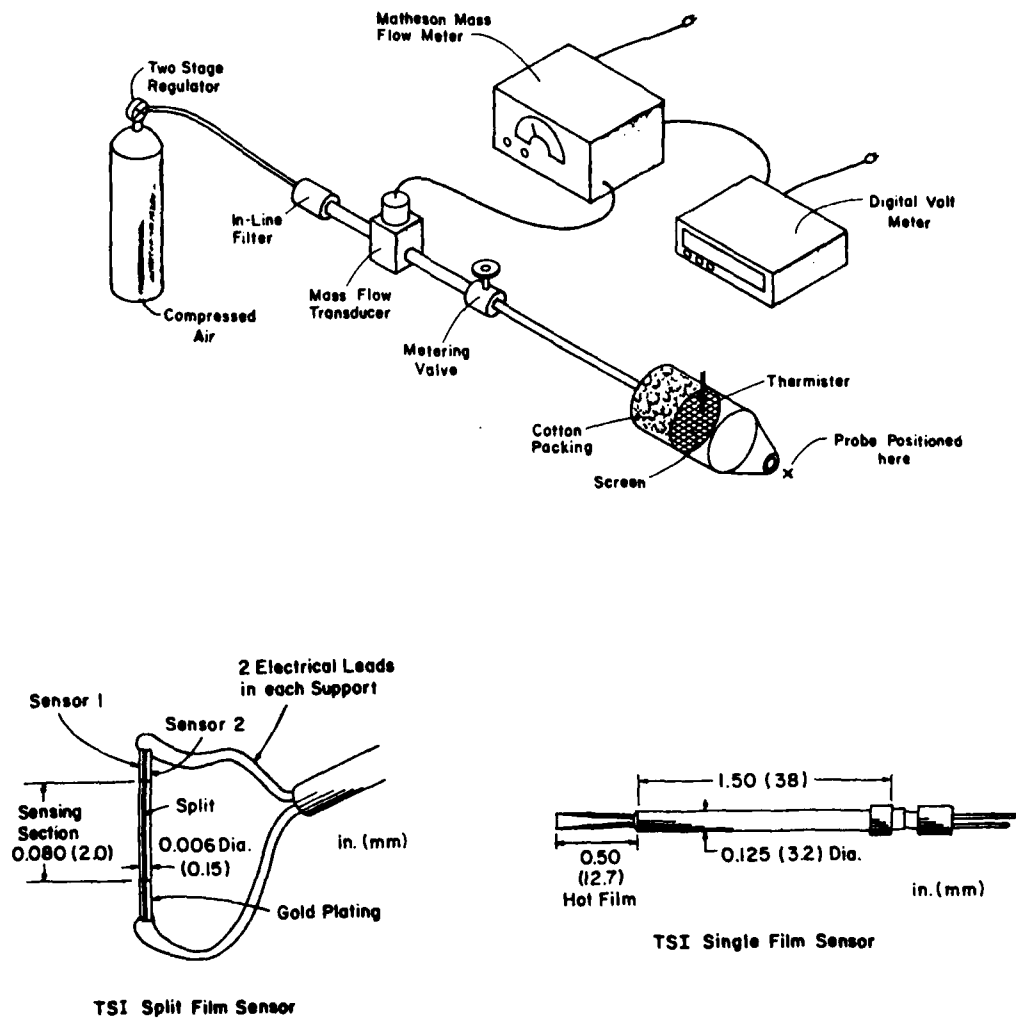


Figure 9. Velocity Probes and Velocity Standard

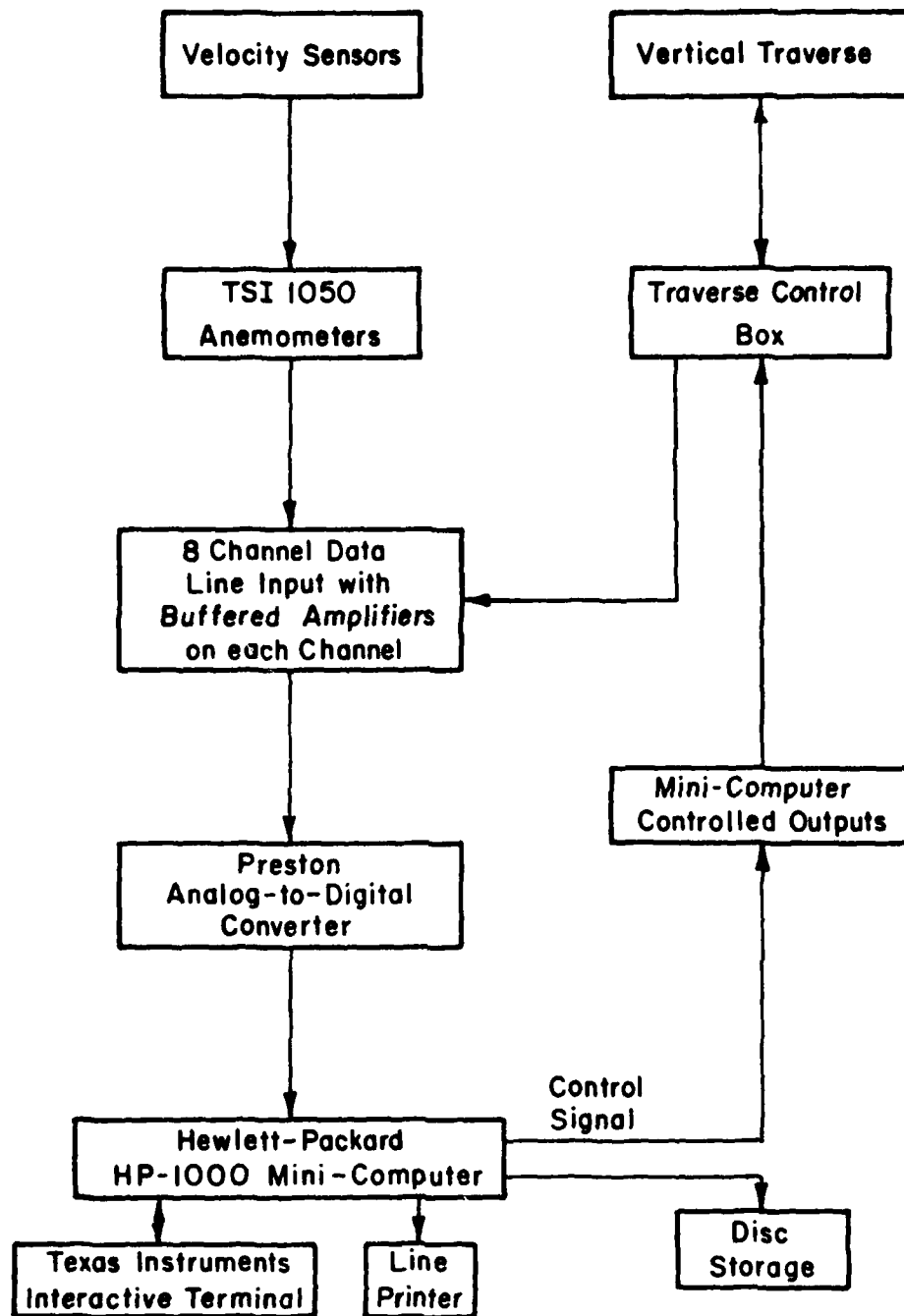


Figure 10. Velocity Data Reduction Flow Chart

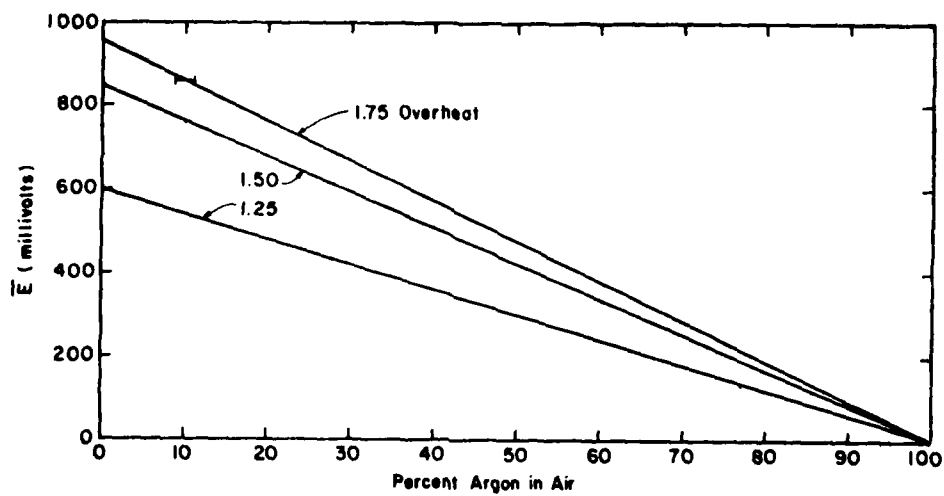


Figure 11. Typical Response of Hot Film Aspirating Probe

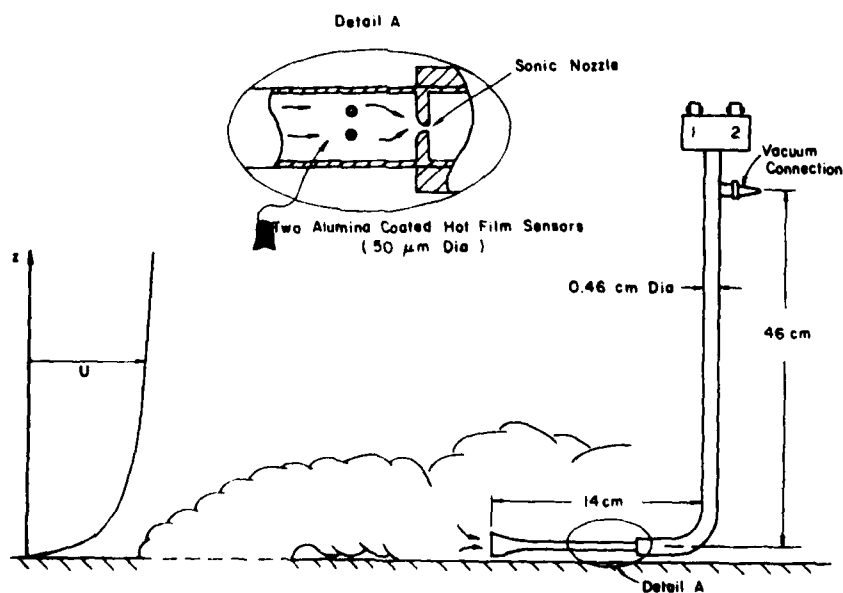


Figure 12. Hot Film Aspirating Concentration Probe

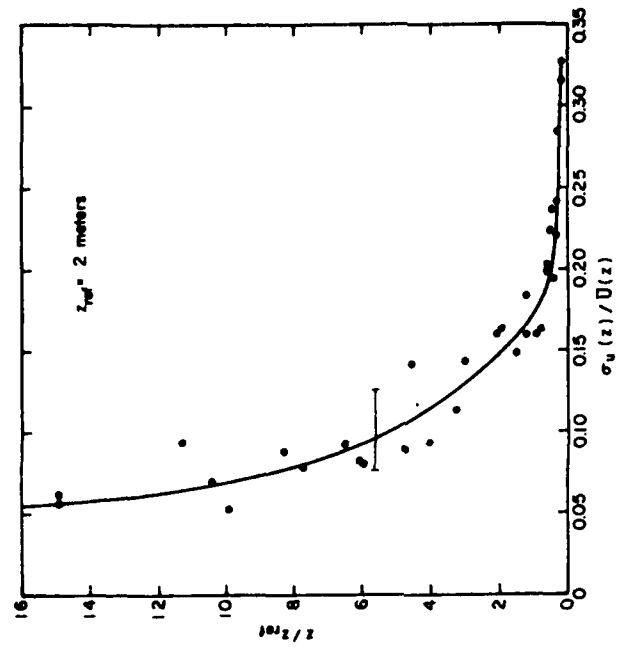


Figure 14. Local Longitudinal Turbulent Intensity Profile

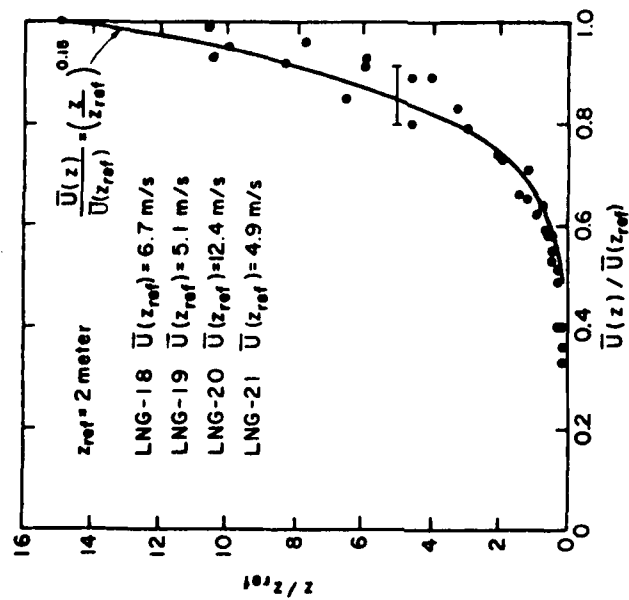


Figure 13. Velocity Profiles

Test-Run No. 3-1  
(No. of Grid Points = 39)

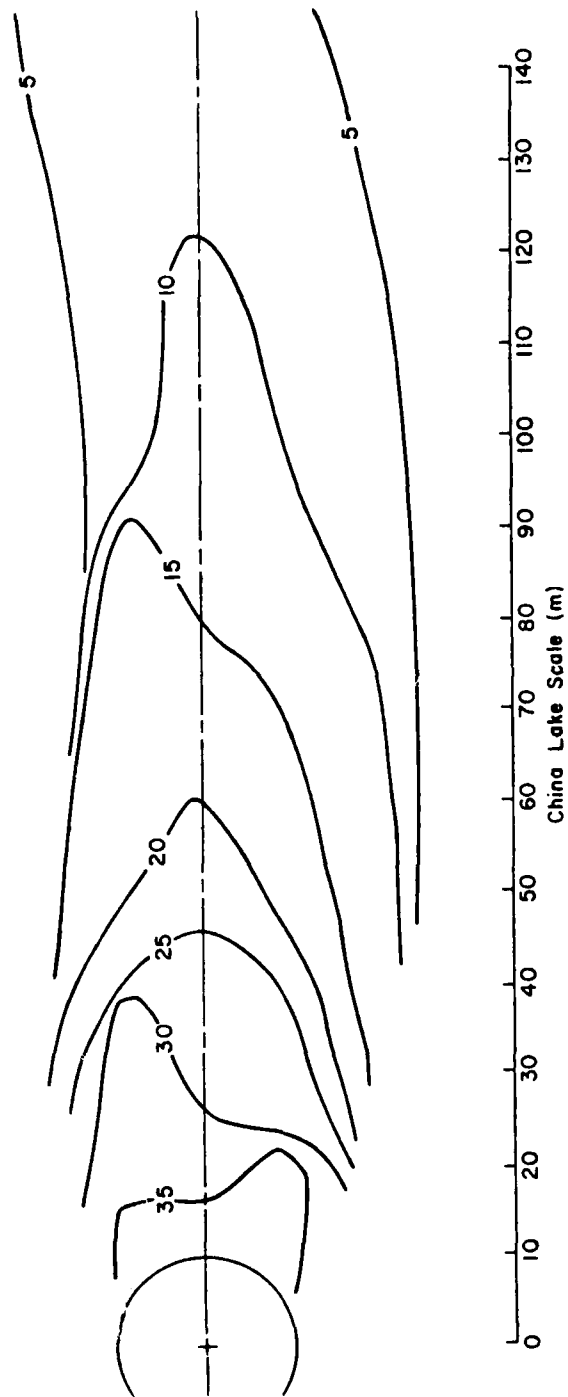


Figure 15-1. Ground Contour Plot of Peak Concentration

Test-Run No. 3-2  
(No. of Grid Points = 20)

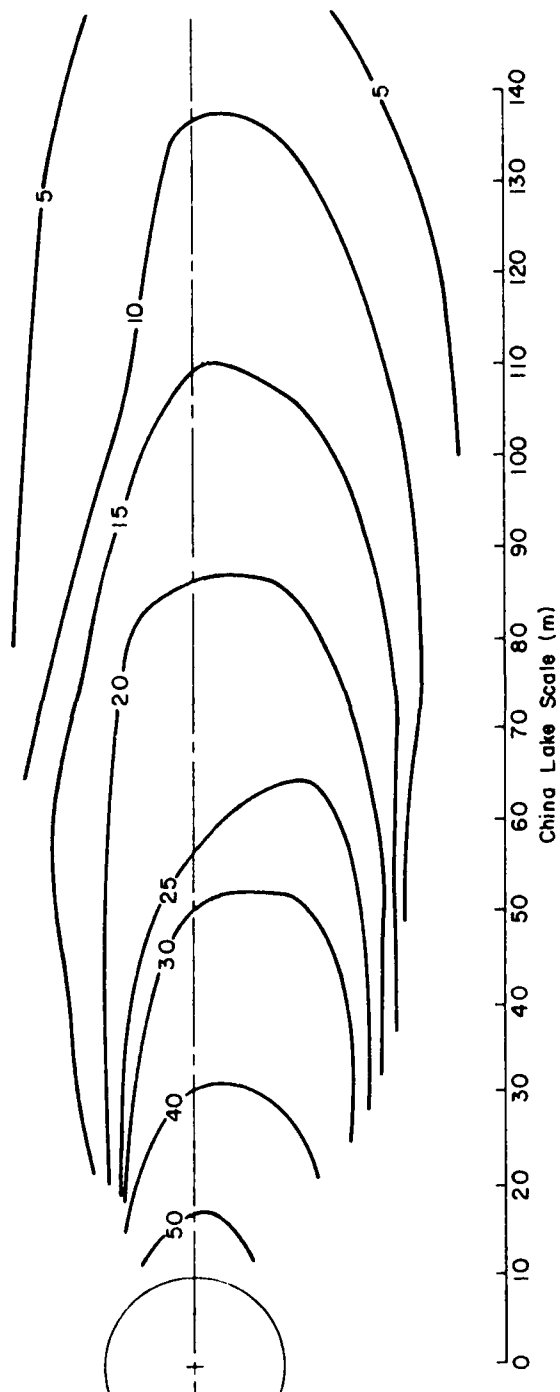
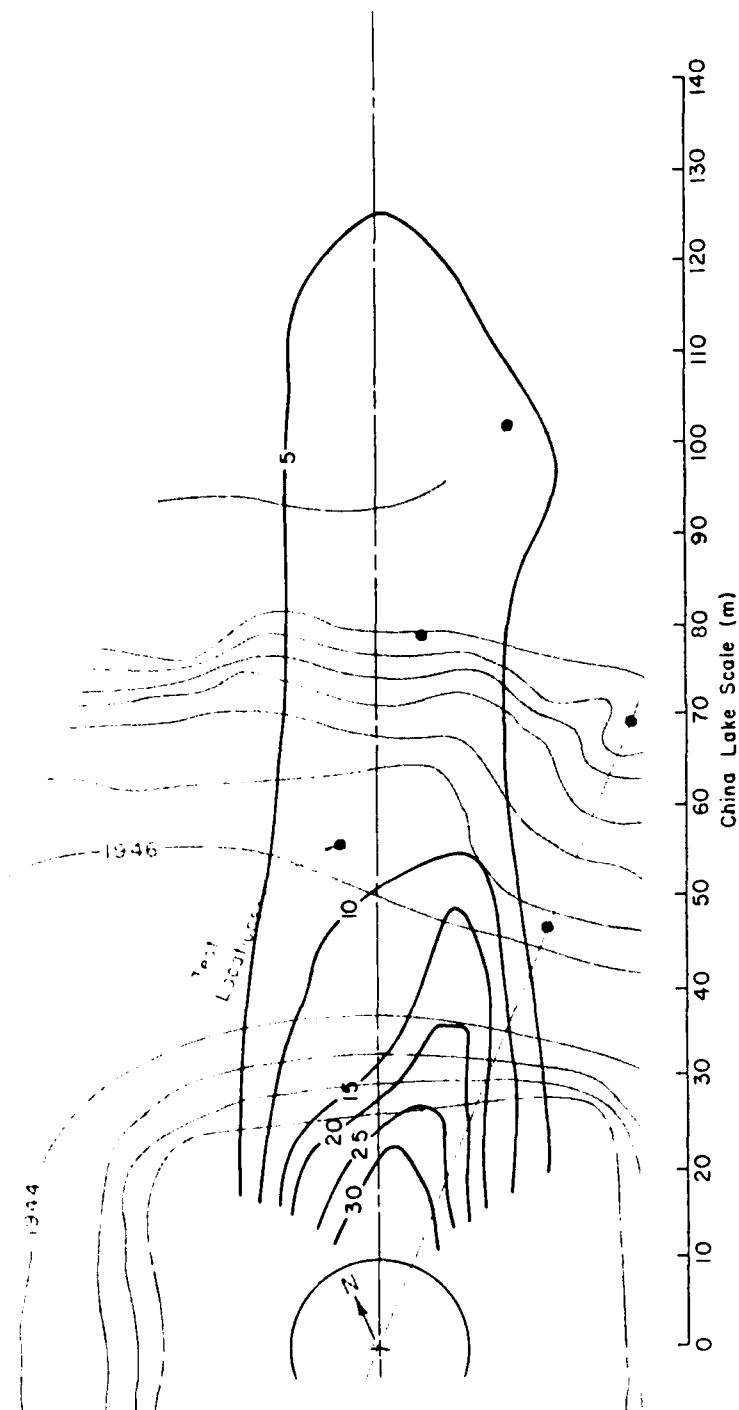


Figure 15-2. Ground Contour Plot of Peak Concentration



Test-Run No. 3-3  
(No. of Grid Points = 55)



Test-Run No. 3-4  
(No. of Grid Points = 56)

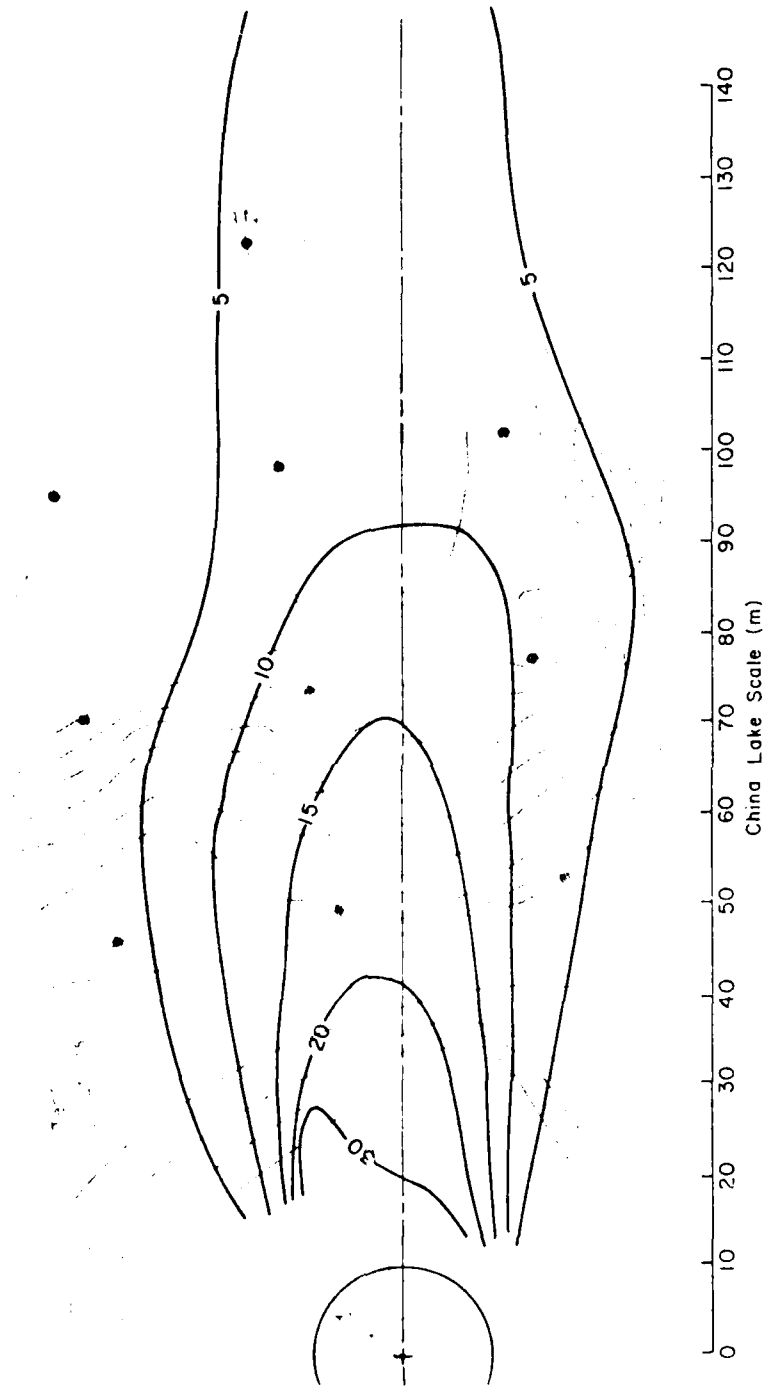


Figure 15-4. Ground Contour Plot of Peak Concentration

Test-Run No. LNG-18  
 (No. of Grid Points = 18)  
 Circled Numbers are LLL Field Values

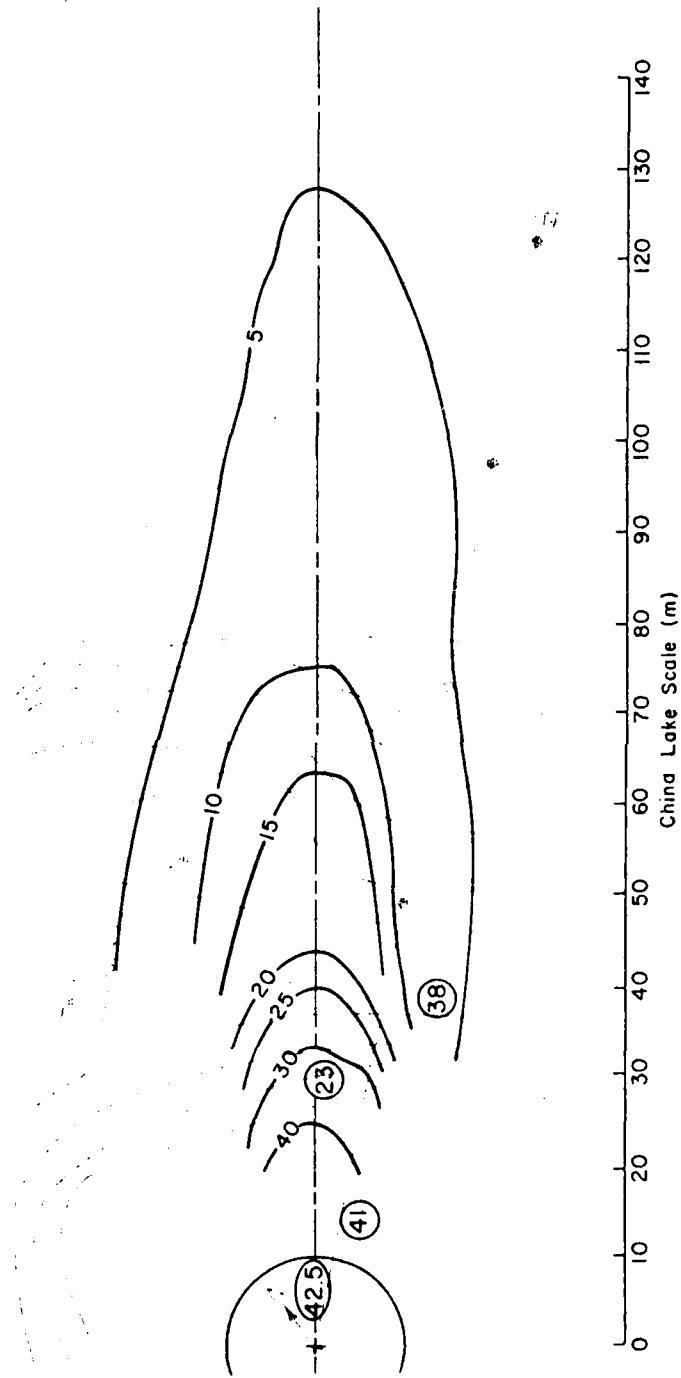


Figure 15-5. Ground Contour Plot of Peak Concentration

Test-Run No. LNG-19  
 (No. of Grid Points = 12)  
 Circled Numbers are LLL Field Values

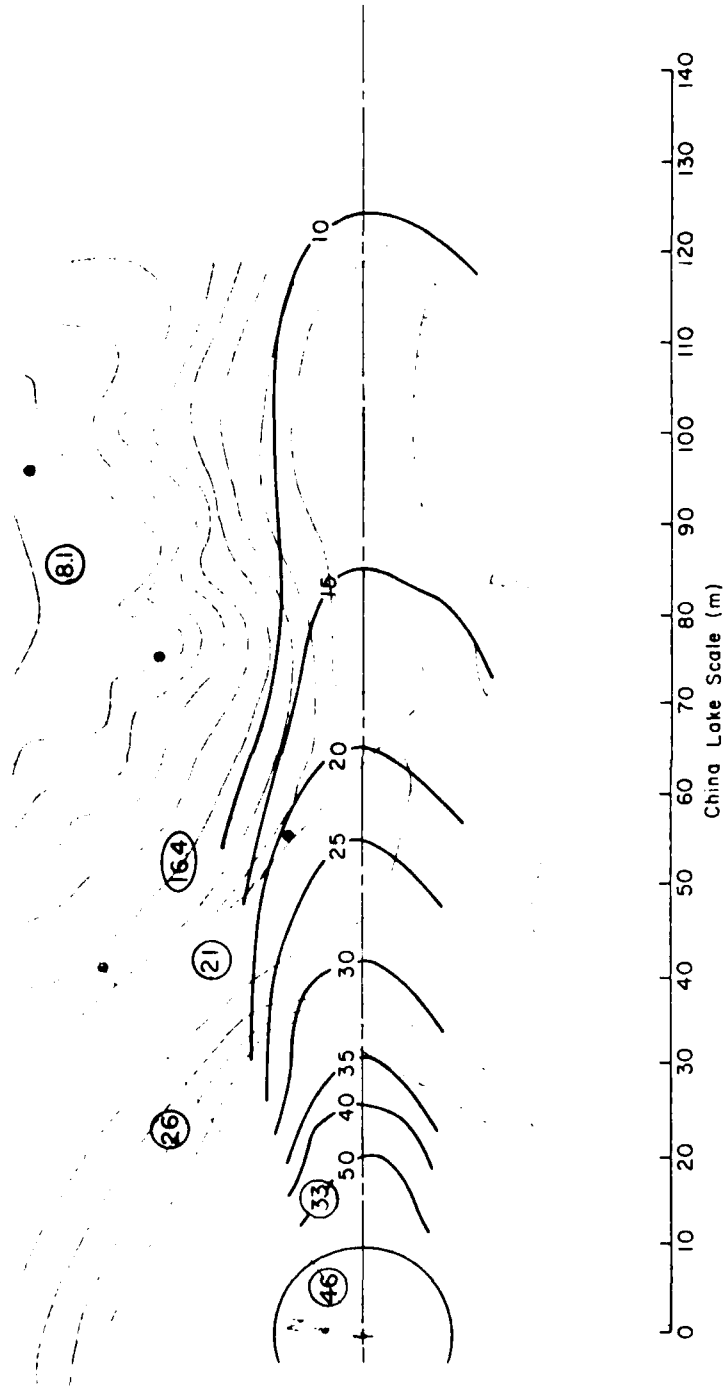


Figure 15-6. Ground Contour Plot of Peak Concentration

Test-Run No. LNG-20  
(No. of Grid Points = 47)  
Circled Numbers are LLL Field Values

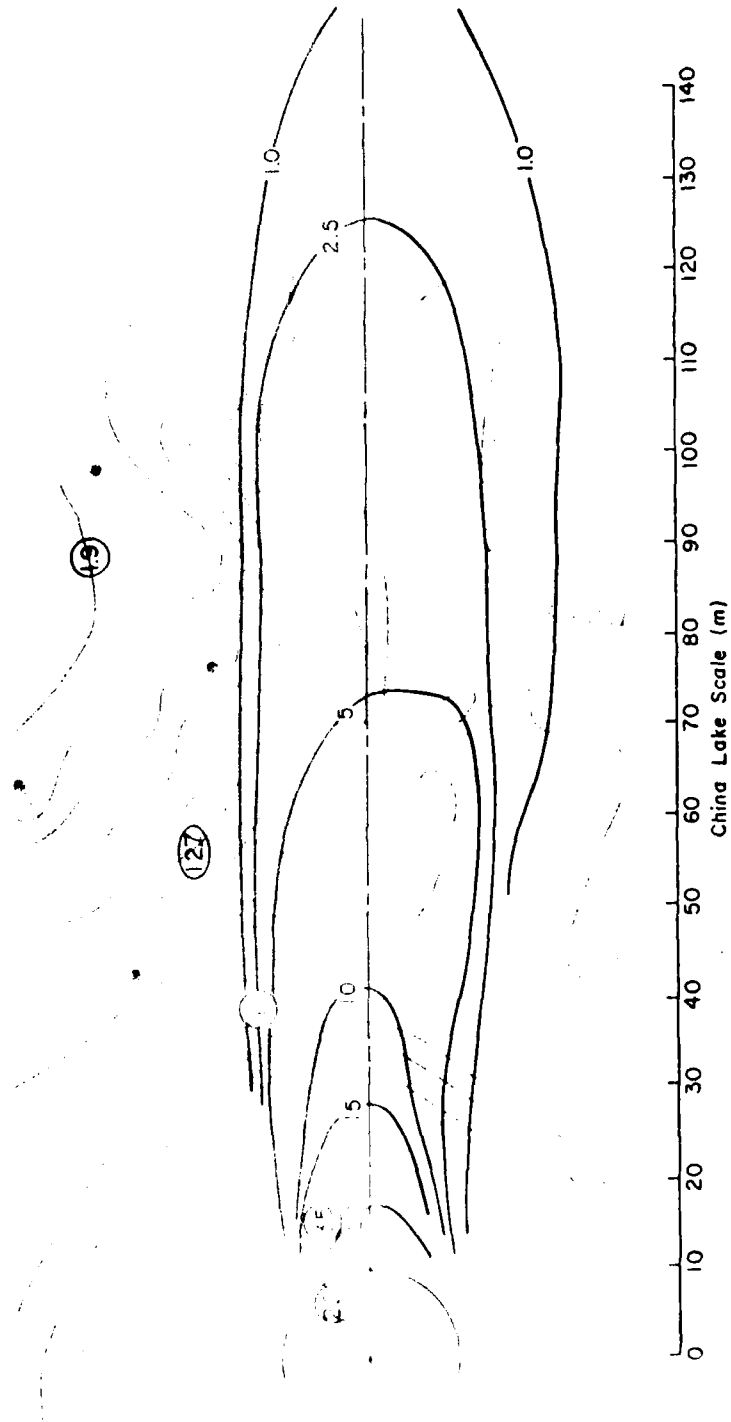


Figure 15-7. Ground Contour Plot of Peak Concentration

Test Run No. LNG-21  
 (No. of Grid Points = 91)  
 Circled Numbers are LLL Field Values

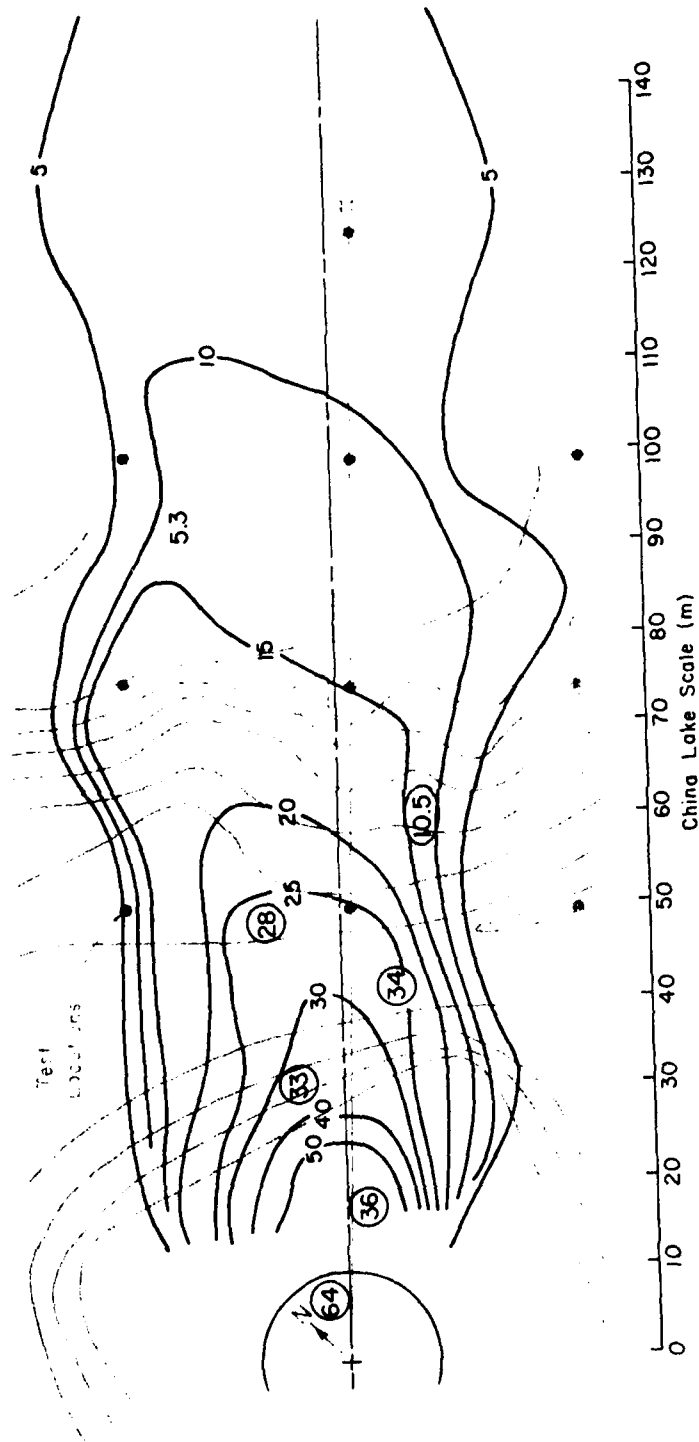


Figure 15-8. Ground Contour Plot of Peak Concentration

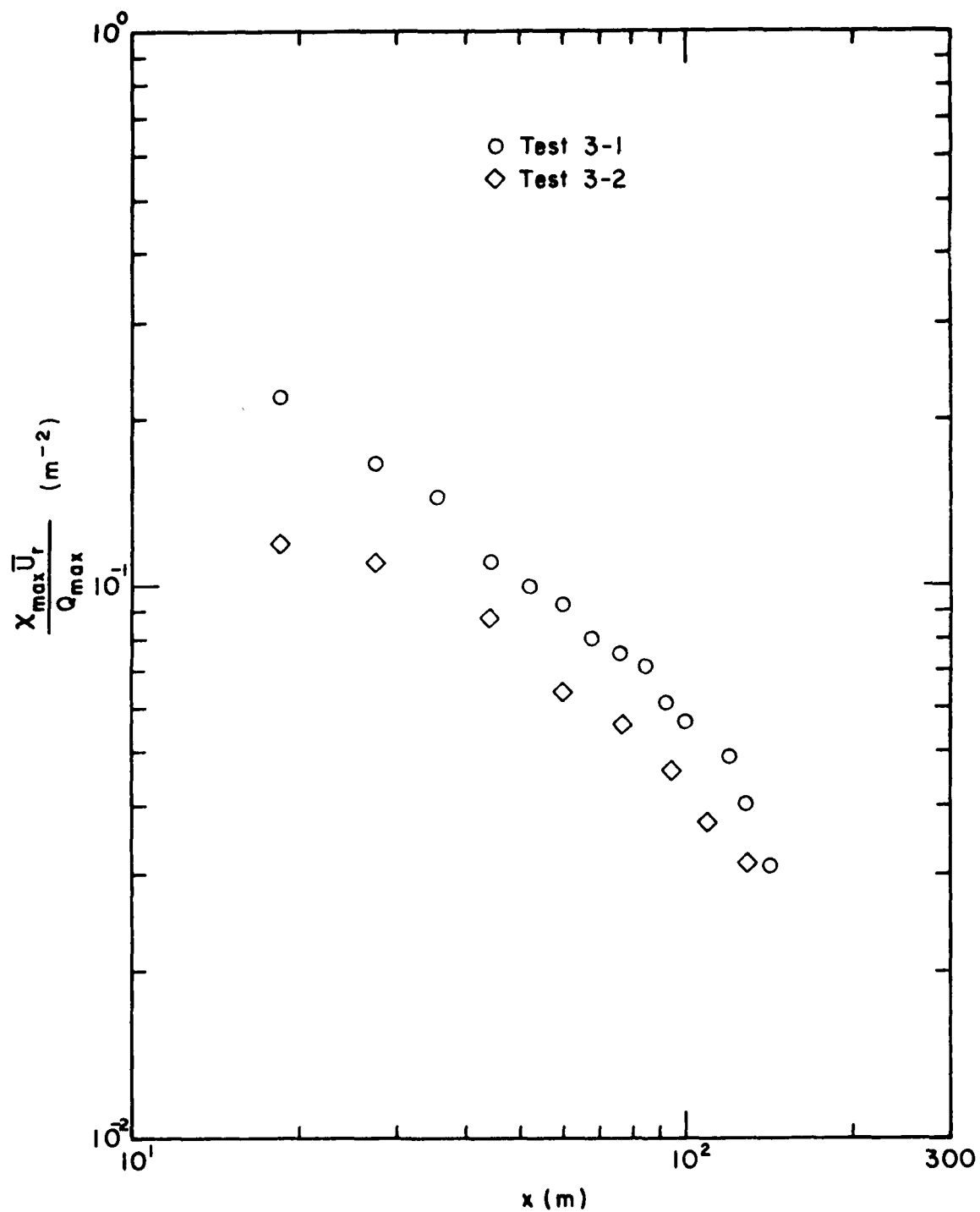


Figure 16-1. Normalized Concentration Versus Downwind Distance

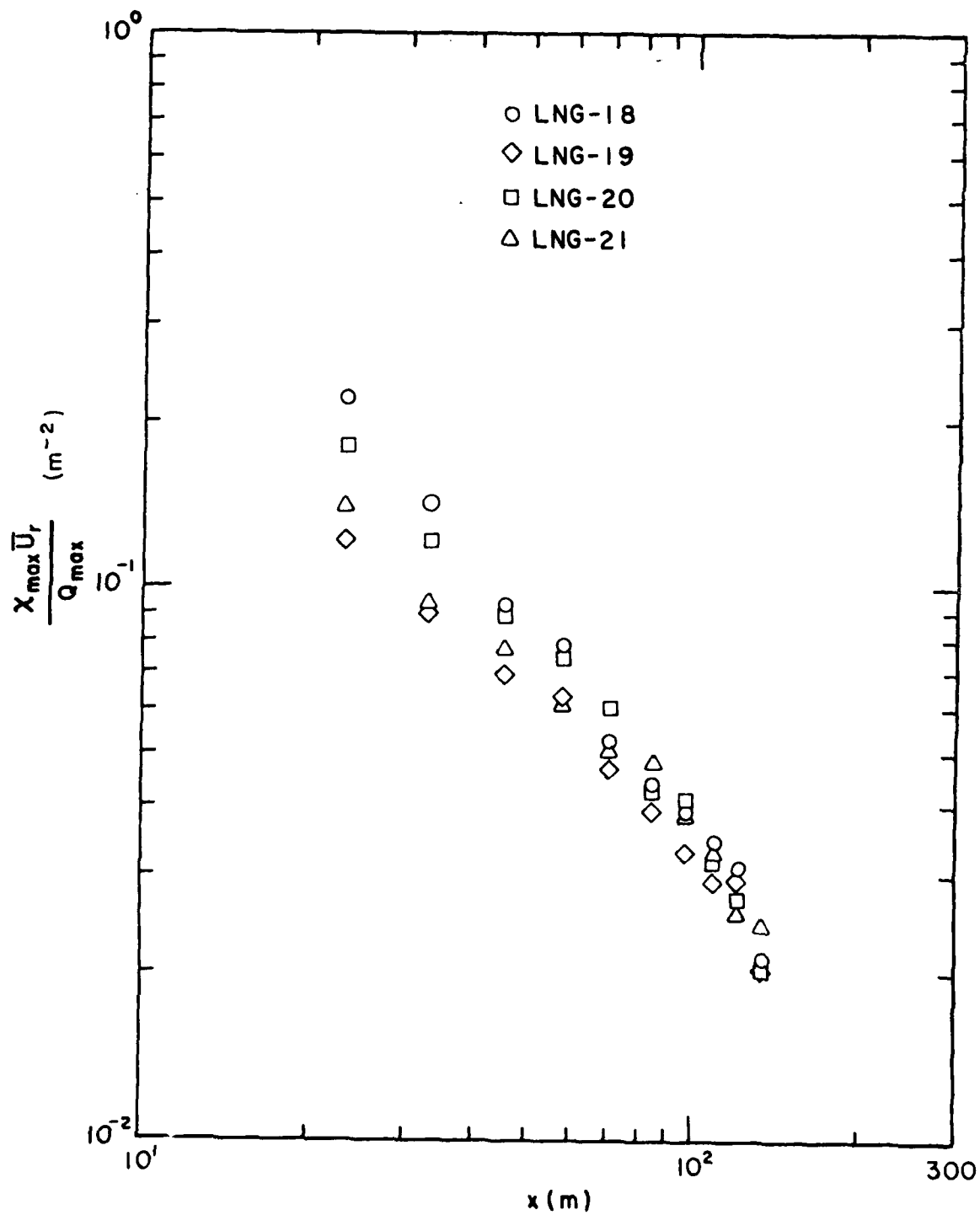


Figure 16-2. Normalized Concentration Versus Downwind Distance



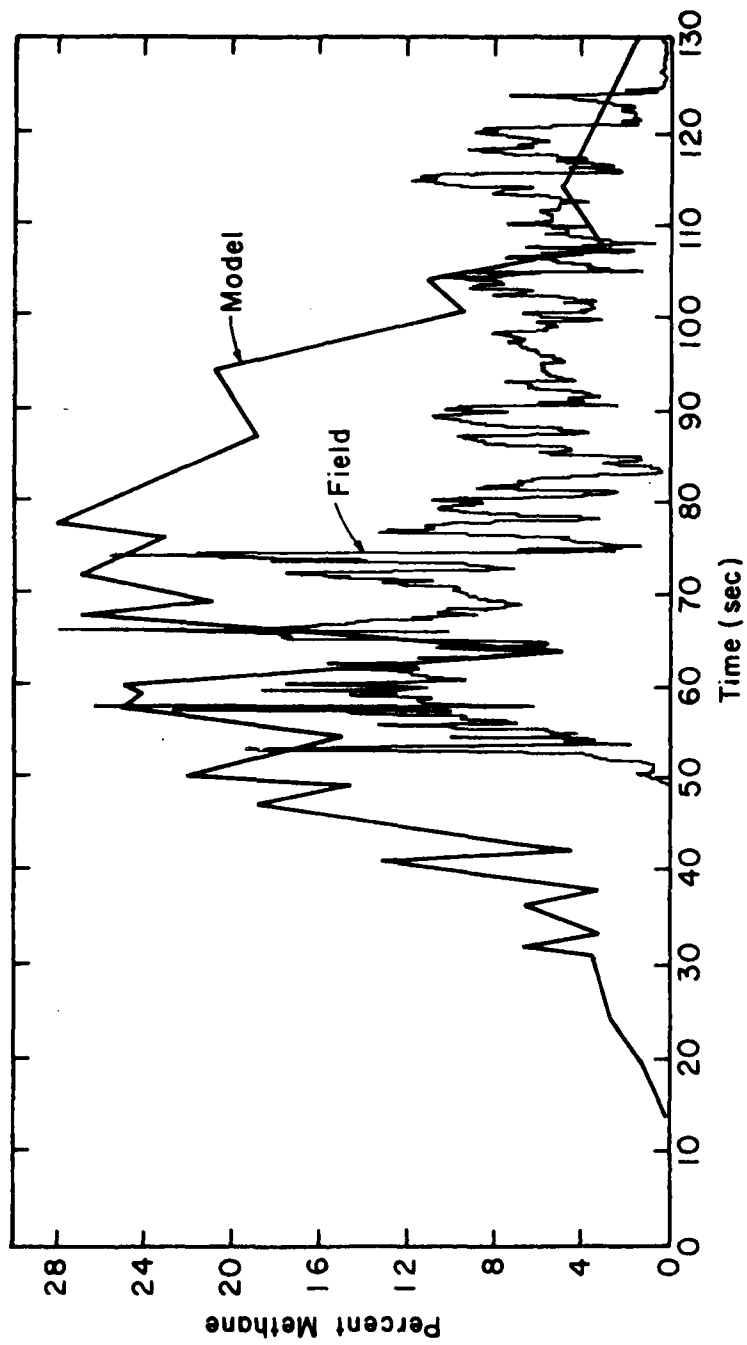


Figure 17. Concentration Comparison For LLL Grid Point 5 For Test LNG-21.

## APPENDIX A - The Calculation of Model Scale Factors

As discussed previously in Section 2.3 the dominant scaling criterion for the simulation of LNG vapor cloud physics are the Froude number and the volume flux ratio. By setting these parameters equal for model and prototype one obtains the following relationships for a model (length scale (L.S.) of 1:85 and a model specific gravity (S.G.) of 1.38

$$(U_a)_m = \left( \frac{S.G._m - 1}{S.G._p - 1} \right)^{1/2} \left( \frac{1}{L.S.} \right)^{1/2} (U_a)_p = 0.090 (U_a)_p$$

$$Q_m = \left( \frac{S.G._m - 1}{S.G._p - 1} \right)^{1/2} \left( \frac{1}{L.S.} \right)^{2.5} Q_p = (1.25 \times 10^{-5}) Q_p$$

$$t_m = \left( \frac{S.G._p - 1}{S.G._m - 1} \right)^{1/2} \left( \frac{1}{L.S.} \right)^{0.5} t_p = (0.131) t_p$$

$$L_m = \left( \frac{1}{L.S.} \right) L_p = (0.012) L_p$$

In addition to these scaling parameters which govern the flow physics one must also scale the mole fractions (concentrations) measured in the model to those that would occur in the prototype. This scaling is required since the number of moles being released in a thermal plume are different than the number of moles being released in an isothermal plume. To be more precise the relationship between the molal flow rate of source gas in the model and the prototype is

$$n_p = (T_m/T_p)_{@ \text{ b.o. }} n_m = (2.70) n_m$$

By definition the concentration of LNG vapor is expressed as:

$$x_p = n_{NG} / (n_{NG} + n_a)$$

Substituting model equivalents into the above expression yields

$$x_p = \frac{(T_m/T_p)_{@ \text{ b.o. }} n_{Ar}}{(T_m/T_p)_{@ \text{ b.o. }} n_{Ar} + n_a} = \frac{n_{Ar}}{n_{Ar} + n_a (T_p/T_m)_{@ \text{ b.o. }} }$$

or

$$x_p = \frac{x_m}{x_m + (1 - x_m)(0.37)}$$

This equation was used to correct the modeled measurements to those that would be observed in the field.

**DATE  
FILMED**

**6-8**